Fermi National Accelerator Laboratory

Fermilab-Pub-85/168-T
November, 1985

THE PHASE STRUCTURE OF AN $SU(2)$ LATTICE GAUGE-HIGGS SYSTEM AT ZERO AND FINITE TEMPERATURE

J. C. Sexton

Fermi National Accelerator Laboratory
P. O. Box 500, Batavia, IL 60510

ABSTRACT

The phase structure of an $SU(2)$ lattice gauge system which interacts with Higgs fields transforming under the fundamental representation of the gauge group is obtained with mean field and Monte Carlo methods. If the Higgs four-point coupling λ is large this theory exhibits a second order phase transition for large values of the inverse gauge coupling β which does not, however, divide the parameter space into disjoint phases. As λ decreases this transition extends to the $\beta = 0$ edge parameter space and becomes first order for part of its length. The finite temperature behaviour of the theory is also examined. The phase transition line identified in the zero temperature case appears to be a temperature independent feature of the model. However, study of the Wilson line operator indicates that there is a deconfining transition present in the Higgs symmetric phase of the theory which scales according to the gauge coupling renormalization group equation.

Operated by Universities Research Association Inc. under contract with the United States Department of Energy

1 Introduction

In the past few years the lattice approach to the study of non-perturbative effects in pure non-abelian gauge theories has achieved some remarkable successes. For the case of $SU(3)$, for example, the observables measured have included the deconfining temperature [1], the latent heat of deconfinement [2], the hadronic mass spectrum [3], and the hadronic coupling constants [4]. These calculations suggest that lattice techniques may in the future become the premier tool for the non-perturbative study of a wide variety of different theories.

There are, however, a number of technical problems to be solved before this possibility is realised. Pure non-abelian gauge theories are among the simplest systems to model on the lattice both because the numerical methods needed are quite straightforward and because the continuum limit is well understood. However, when one introduces dynamical particle fields into the problem things become much more difficult. If the fields introduced are scalar fields then the asymptotic freedom of the pure gauge system is destroyed [5] and one no longer understands the connection between the lattice and the continuum. If fermions are introduced then the non-local nature of the fermion interactions increases the magnitude of the numerical simulation required a hundredfold. Fermions on the lattice also suffer from the notorious doubling problem [6] which obscures the chiral symmetry that is such an important feature in many of the systems that we would like to study non-perturbatively.

In this paper we shall begin to address some of these points. The particular system which we shall study consists of an $SU(2)$ gauge field interacting with a complex Higgs doublet. This system is numerically very simple to examine because there are relatively few degrees of freedom involved on any given lattice site and because there exist algorithms which efficiently deal with the importance sampling that is such a crucial feature of the lattice method.

More importantly, however, the system has an extremely rich structure and can with some simple modifications be used to address almost all of the problems which we need to answer. The presence of dynamical particle fields allows us to study the

effects that such fields introduce onto the lattice. Also, if we are content to treat fermions in the quenched approximation, then for weak gauge coupling this model allows us to study symmetry breaking effects like those which occur in the standard model [7], while for strong gauge coupling we can study some of the confinement effects which are so important in preon theories [8].

In the present paper we shall confine our attention to the gauge-Higgs sector only. This study is a necessary prerequisite to the study of the more complex gauge-Higgs-fermion system. We hope to address this latter case in the quenched fermion approximation in a future paper.

The plan of this paper is as follows. Section 2 presents the details of the model and introduces our notation. Section 3 discusses a number of limiting cases which can arise for special choices of the coupling constants. The properties of these limiting cases are well understood and therefore provide a reference for the results which we shall derive later. Section 4 examines the model in the mean field approximation. Section 5 discusses some novel features of the Monte Carlo algorithm which we have used. Section 6 presents the results we have obtained from the Monte Carlo analysis of the model. Finally, Section 7 presents our conclusions.

2 The Model

We shall work throughout on a four dimensional Euclidian lattice with periodic boundary conditions. Sites on the lattice will be denoted by the four-vector $x = (x^0, x^1, x^2, x^3)$, with components x^μ chosen to be integer multiples of the lattice spacing a. Periodic boundary conditions are imposed by identifying sites with components x^μ and $x^\mu + L^\mu$, where L^μ is the length of the lattice in the μth direction. Fundamental links on the lattice are directed line segments connecting sites which are separated by exactly one lattice spacing. We shall denote such links by the ordered pair $(x, x \pm \hat{\mu})$ where x and $x \pm \hat{\mu}$ are respectively the source and sink sites of the link and where $\hat{\mu}$ is a vector of length a directed along the positive μ-axis of the lattice. For notational convenience we shall generally set $a = 1$.

The basic fields of the theory are the gauge fields $U(x, x \pm \hat{\mu})$ defined on the links

of the lattice and the Higgs fields $W(x)$ defined on the sites. Each gauge field is an $SU(2)$ matrix constrained so that $U(x,x+\hat{\mu}) = U^\dagger(x+\hat{\mu},x)$. Introduce the matrix four-vector $\Sigma = (1, i\vec{\sigma})$, where $\vec{\sigma} = (\sigma^1, \sigma^2, \sigma^3)$ are the Pauli matrices. We can then parameterize $U(x,x+\hat{\mu})$ as

$$U(x,x+\hat{\mu}) \;=\; u^\alpha(x,x+\hat{\mu})\Sigma^\alpha \;=\; u^0(x,x+\hat{\mu}) + i\vec{u}(x,x+\hat{\mu})\cdot\vec{\sigma} \qquad (2.1)$$

where the components u^α are real, and $det(U) = u^\alpha u^\alpha = 1$.

The particular form we adopt for the Higgs fields depends on the representation under which those fields transform. Fundamental $SU(2)$ Higgs fields are usually denoted by a two-component complex scalar field ϕ^a, $a = 1,2$. We shall, however, choose to decompose ϕ into its real and imaginary parts. Thus the Higgs field will be denoted by a four-component real field $w^\alpha(x)$, $\alpha = 0\ldots3$. Further, we shall make use of the matrices Σ^α defined above to write this field as a 2×2 complex matrix $W(x)$ as follows

$$W(x) \;=\; w^\alpha(x)\Sigma^\alpha \;=\; w^0(x) + i\vec{w}\cdot\vec{\sigma} \qquad (2.2)$$

Thus, the gauge and Higgs fields have the same form, except that the gauge fields are constrained to have unit determinant while the Higgs field determinant can have any positive value. In terms of the Higgs doublet ϕ, $W(x)$ decomposes as

$$W(x) \;=\; \begin{pmatrix} w^0 + iw^3 & iw^1 + w^2 \\ iw^1 - w^2 & w^0 - iw^3 \end{pmatrix} \;=\; \sqrt{2}\begin{pmatrix} \phi^1 & -\phi^{2\dagger} \\ \phi^2 & \phi^{1\dagger} \end{pmatrix} \qquad (2.3)$$

The action S which we shall study is given by

$$\begin{aligned} S &= S_G + S_H \\ S_G &= \sum_{x,\mu<\nu} \beta \left(1 - \tfrac{1}{2}Tr\left[U_\Box(x,\mu,\nu)\right]\right) \\ S_H &= \sum_x \lambda \left(\tfrac{1}{2}Tr\left[W^\dagger(x)W(x)\right] - \gamma\right)^2 \\ &\quad + \sum_x 4 \left(\tfrac{1}{2}Tr\left[W^\dagger(x)W(x)\right]\right) \\ &\quad - \sum_{x,\mu} \left(\tfrac{1}{2}Tr\left[W^\dagger(x)U(x,x+\hat{\mu})W(x+\hat{\mu})\right]\right) \end{aligned} \qquad (2.4)$$

In S_G the sum is over all unoriented plaquettes, while $U_\Box$ denotes the path-ordered product around the appropriate plaquette of the gauge matrices sitting on the links of that plaquette

$$U_\Box(x,\mu,\nu) = U(x,x+\hat{\mu})U(x+\hat{\mu},x+\hat{\mu}+\hat{\nu})U(x+\hat{\mu}+\hat{\nu},x+\hat{\nu})U(x+\hat{\nu},x) \tag{2.5}$$

This action exhibits two different $SU(2)$ symmetries. The first, the local $SU(2)$ gauge symmetry, is defined by the transformations

$$\begin{aligned} U(x,x+\hat{\mu}) &\rightarrow g(x)U(x,x+\hat{\mu})g^\dagger(x+\hat{\mu}) \\ W(x) &\rightarrow g(x)W(x) \end{aligned} \tag{2.6}$$

where the transformation matrices $g(x)$ are $SU(2)$ matrices. The second $SU(2)$ symmetry is a global symmetry of the Higgs sector defined by

$$W(x) \rightarrow W(x)h^\dagger \tag{2.7}$$

where h is a constant $SU(2)$ matrix. This latter symmetry is a consequence of the fact that the Higgs sector has an $O(4) \approx SU(2) \otimes SU(2)$ symmetry when the gauge interactions are turned off.

To generate the naive continuum limit of the action of Eqn.(2.4) we make the following transcriptions

$$\begin{aligned} U(x,x+\hat{\mu}) &\rightarrow \exp\left(iga\vec{A}^\mu(x)\cdot\frac{\vec{\sigma}}{2}\right) \\ W(x) &\rightarrow \sqrt{2}\,a\begin{pmatrix} \phi_c^1 & -\phi_c^{2\dagger} \\ \phi_c^2 & \phi_c^{1\dagger} \end{pmatrix} \\ \beta &\rightarrow \frac{4}{g^2} \\ \gamma &\rightarrow -\frac{m^2a^2}{4\lambda} \end{aligned} \tag{2.8}$$

The limit $a \rightarrow 0$ is now straightforward. The action which results is

$$\begin{aligned} S &\rightarrow \int d^4x\ \frac{1}{4}\vec{F}^{\mu\nu}\cdot\vec{F}^{\mu\nu} \\ &+ \int d^4x\ (D^\mu\phi_c)^\dagger(D^\mu\phi_c) + m^2\phi_c{}^\dagger\phi_c + 4\lambda(\phi_c{}^\dagger\phi_c)^2 \end{aligned} \tag{2.9}$$

where

$$\begin{aligned} \vec{F}^{\mu\nu} &= \partial^\mu \vec{A}^\nu - \partial^\nu \vec{A}^\mu - g\vec{A}^\mu \times \vec{A}^\nu \\ D^\mu &= \partial^\mu + ig\vec{A}^\mu \cdot \frac{\vec{\sigma}}{2} \end{aligned} \tag{2.10}$$

This continuum form describes an $SU(2)$ gauge field $\vec{A}^\mu$ interacting with a complex Higgs doublet ϕ_c. Thus we identify g, 4λ, and m^2 as, respectively, the gauge, the Higgs quartic, and the Higgs quadratic bare couplings for an $SU(2)$ gauge theory coupled to a single complex scalar doublet. Note also that choosing $m^2 > 0$ ($\gamma < 0$) results in a non-abelian generalization of scalar QED, while $m^2 < 0$ ($\gamma > 0$) is the spontaneous symmetry breaking choice.

3 Limiting Models

The action which we have written down in Eqn.(2.4) is a function of three independent parameters: the gauge coupling β, and the Higgs couplings λ and γ. These three parameters define a three dimensional space with limits: $0 \leq \beta < \infty$, $0 < \lambda < \infty$, and $-\infty < \gamma < \infty$. We are, of course, interested in determining the phase structure of this action for general values of these parameters. However, before considering the general problem, it is instructive to review some standard results which apply for certain special choices.

3.1 The Pure Higgs Limit: $\beta \to \infty$

If we take $\beta \to \infty$ then, for each plaquette, $\frac{1}{2}Tr\,[U_\Box] \to 1$. Thus the gauge fields are frozen to pure gauge configurations and we can, without loss of generality, set all the U's equal to the identity. Then, in component notation (Eqn.(2.2)), the action becomes

$$\begin{aligned} S_H \;\to\; & \sum_{x,\mu} \left(w^\alpha(x)w^\alpha(x) - w^\alpha(x)w^\alpha(x+\hat{\mu})\right) \\ + \; & \sum_x \lambda \left(w^\alpha(x)w^\alpha(x) - \gamma\right)^2 \end{aligned} \tag{3.1}$$

This action describes a four-dimensional spin model with an O(4) global symmetry. It has a particularly simple form if we take $\lambda \to \infty$ with γ held fixed and positive. This limit freezes the magnitude of the Higgs fields w^α to $w^\alpha w^\alpha \to \gamma$ and, after

rescaling, the action becomes

$$S_H \rightarrow -\gamma \sum_{x,\mu} \hat{w}^\alpha(x)\hat{w}^\alpha(x+\hat{\mu}) \tag{3.2}$$

where

$$w^\alpha(x) = \sqrt{\gamma}\,\hat{w}^\alpha(x) \tag{3.3}$$

Eqn.(3.2) describes an O(4) four-dimensional generalized Heisenberg model with γ playing the role of inverse temperature.

The phase structure for the Heisenberg model is well understood [9]. Providing the dimension d is greater than the critical dimension $d = 2$, two phases will be present. When γ is sufficiently large the Higgs field develops a vacuum expectation value, and the $O(4)$ global symmetry is spontaneously broken. Because of the presence of massless Goldstone modes, the correlation function $\langle \hat{w}^\alpha(0)\hat{w}^\alpha(r)\rangle$ has the asymptotic behaviour

$$\lim_{r\to\infty} \langle \hat{w}^\alpha(0)\hat{w}^\alpha(r)\rangle \rightarrow \exp\left(-\frac{\text{const}}{r}\right) \tag{3.4}$$

In particular we note that the long-range correlation is nonzero, indicating symmetry breaking in this phase. On the other hand, when γ is small, the global symmetry remains unbroken, there are no massless excitations, and the correlation function decays exponentially. Further, the transition between the two phases is second order.

For γ nonzero and finite, we expect no qualitative changes in this picture. γ no longer has the interpretation of an inverse temperature, but we still expect that no matter how small we make λ, we can always choose γ sufficiently large so that the potential term, $\lambda\gamma^2\left(\hat{w}^\alpha\hat{w}^\alpha - 1\right)^2$ freezes $\langle \hat{w}^\alpha\hat{w}^\alpha\rangle \rightarrow 1$. Then, to show that a Higgs phase must always be present, we make use of an infrared bound due to Frohlich and Simon [10]. For the action of Eqn.(3.1), this bound takes the form

$$\lim_{r\to\infty} \langle \hat{w}^\alpha(0)\hat{w}^\alpha(r)\rangle \geq \langle \hat{w}^\alpha(0)\hat{w}^\alpha(0)\rangle - \frac{\text{const}}{\gamma} \tag{3.5}$$

Thus, for γ sufficiently large, the right hand side of this inequality will be positive definite, and the Higgs symmetry will be broken.

3.2 The Pure Gauge Limit: $\gamma \to -\infty$

If $\gamma < 0$ we can rewrite the Higgs potential as

$$\lambda \left(w^\alpha w^\alpha - \gamma\right)^2 = \lambda \left(\left(w^\alpha w^\alpha\right)^2 + 2\left|\gamma\right| w^\alpha w^\alpha + \gamma^2 \right) \tag{3.6}$$

Then, taking $\gamma \to -\infty$ forces $w^\alpha \to 0$, since the term $2\left|\gamma\right| w^\alpha w^\alpha$ gives very large action to all configurations with w^α non zero. Therefore, in this limit, the Higgs field drops completely from the problem, and the action reduces to that for a pure $SU(2)$ gauge theory

For space time dimension $d = 4$, this action has a single confining phase for all values of β [11]. The theory does, however, exhibit a crossover at $\beta \approx 2.2$ which separates the regions where strong coupling (small β) expansions and weak coupling (large β) expansions are valid. For $d > 4$, this crossover turns into a first order phase transition [11]. The small β sector remains confining, but for large β confinement disappears. Instead, the large β phase exhibits Coulomb forces between static charges.

3.3 The Limit: $\beta \to 0$

This limit is more easily analyzed if we transform to the unitary gauge. To define this gauge transformation, first decompose the Higgs field $W(x)$ into a radial field $\rho(x)$ and an $SU(2)$ spin field $V(x)$. The fields ρ and V are defined by

$$\begin{aligned} \rho(x) &= \sqrt{det\left(W(x)\right)} = \sqrt{\left(w^\alpha w^\alpha\right)} \\ W(x) &= \rho(x)\, V(x) \end{aligned} \tag{3.7}$$

The unitary gauge transformation is then given by

$$\begin{aligned} U(x, x+\hat{\mu}) &\to V(x) U(x, x+\hat{\mu}) V^\dagger(x+\hat{\mu}) \\ W(x) &\to W(x) V^\dagger(x) \end{aligned} \tag{3.8}$$

In the unitary gauge, the action of Eqn.(2.4) takes the form

$$\begin{aligned} S \;\rightarrow\; & \sum_{\square} \beta \left(1 - \tfrac{1}{2} Tr\left[U_{\square}\right]\right) \\ & + \sum_{x,\mu} \left(\rho^2(x) - \rho(x)\rho(x+\hat{\mu}) \tfrac{1}{2} Tr\left[U(x,x+\hat{\mu})\right]\right) \\ & + \sum_{x} \lambda \left(\rho^2(x) - \gamma\right)^2 \end{aligned} \tag{3.9}$$

Setting $\beta = 0$ in Eqn.(3.9) does not usefully simplify this action. There is still coupling between the gauge and the Higgs radial fields even though the gauge self-coupling has disappeared. However, if we also set $\lambda \rightarrow \infty$ then this situation changes. If $\gamma > 0$ then $\rho(x) \rightarrow \sqrt{\gamma}$ while if $\gamma < 0$, we find $\rho(x) \rightarrow 0$. In either case the action becomes completely trivial, and therefore in the combined limit $\beta \rightarrow 0$, and $\lambda \rightarrow \infty$, the theory can have no phase transitions.

3.4 The Limit: $\gamma \rightarrow \infty$

To analyze this limit we shall, as in the last section, make use of the unitary gauge transformation introduced in Eqn.(3.8). It will also be convenient to introduce a rescaled Higgs radial field, $\hat{\rho}(x)$ corresponding to the rescaled Higgs component field $\hat{w}^{\alpha}(x)$ introduced in Eqn.(2.2). The action then takes the form

$$\begin{aligned} S \;\rightarrow\; & \sum_{\square} \beta \left(1 - \tfrac{1}{2} Tr\left[U_{\square}\right]\right) \\ & + \sum_{x,\mu} \gamma \left(\hat{\rho}^2(x) - \hat{\rho}(x)\hat{\rho}(x+\hat{\mu}) \tfrac{1}{2} Tr\left[U(x,x+\hat{\mu})\right]\right) \\ & + \sum_{x} \lambda\gamma^2 \left(\hat{\rho}^2(x) - 1\right)^2 \end{aligned} \tag{3.10}$$

where

$$\rho(x) \;=\; \sqrt{\gamma}\, \hat{\rho}(x) \tag{3.11}$$

Now when we set $\gamma \rightarrow \infty$ two things happen. First the Higgs potential energy term forces $\hat{\rho}(x) \rightarrow 1$. Then the Higgs kinetic energy forces $\frac{1}{2} Tr\left[U(x,x+\hat{\mu})\right] \rightarrow 1$, which in turn sets $U(x,x+\hat{\mu}) \rightarrow 1$, since the Higgs field is in the fundamental representation of $SU(2)$. Thus, all of the fields are frozen in this limit, and the

theory becomes trivial and has no phase transitions. In contrast to the results of the last section, however, we expect the theory to remain trivial in this limit for all choices of λ.

3.5 Higgs — Confinement Complementarity

We can summarize the results of this chapter in the tentative phase diagram of Figure 1. For large β we expect the theory to exhibit a single second order phase transition at some positive value γ. This transition separates a Higgs sector where γ is large and positive from a confining sector where γ is negative. Further, we expect this transition to exist for all finite values of λ. None of the other edges of the phase diagram are expected to have transitions, at least for large λ. Therefore, at some point in the interior of the diagram, the Higgs-confinement transition must disappear and the two phases merge. Indeed, we are forced to conclude that the theory has, in fact, only a single phase since we can move between any two points on the phase diagram without crossing a phase transition [12].

One should note that this result depends critically on the fact that the Higgs field is in the fundamental representation of the gauge group, and that the unitary gauge, therefore, completely breaks the gauge symmetry. If the Higgs field transforms under some other representation of the gauge group, then the argument used in the last section to derive the triviality of the phase structure in the $\gamma \rightarrow \infty$ limit may no longer follow. That argument required that $\frac{1}{2}Tr\,[U] = 1$ imply $U = 1$. If, however, the Higgs field is in the adjoint representation of the gauge group, for example, then requiring $Tr[U] \propto 1$ constrains U so that $U \in Z_2$ where Z_2 is the center of $SU(2)$. Therefore, the $\gamma \rightarrow \infty$ limit in this case reduces the theory to a pure Z_2 gauge theory which does have a non-trivial phase structure, and the phase transition line entering at large β no longer needs to end somewhere in the interior of the model's parameter space. Instead, it can join the transition line which we expect to be entering at large γ where there is a Z_2 phase transition, and the adjoint model can therefore have two distinct phases.

4 The Mean Field Approximation

The basic premise of the lattice mean field approximation is that in a large space-time dimension a particular field will have a large number of neighbours, and therefore will be insensitive to the individual fluctuations of those neighbours. Instead, the field in question will react mainly to the average or mean field generated by all of its neighbours. The mean field approximation is particularly suitable for determining phase structure. One imposes self-consistency to obtain the mean fields as functions of the parameters in the theory. Then phase transitions show up as singularities in the mapping from parameters to mean fields.

4.1 The mean field approximation with no gauge fixing

There are a number of different ways of deriving the mean field approximation [13]. We shall adopt a particularly simple approach which makes use of Peierls' Inequality,

$$\langle \exp\ (\ A\ )\ \rangle\ \ \geq\ \ \exp\ (\ \langle A \rangle\ ) \tag{4.1}$$

to estimate the partition function Z, or equivalently the free energy per site F, defined by the following equations

$$\begin{aligned} Z &= \int \prod_x d[W(x)] \prod_{x,\mu} d[U(x, x+\hat{\mu})]\ \ \exp(-S) \\ F &= \frac{1}{N_s} \ln(Z) \end{aligned} \tag{4.2}$$

where S is the action introduced in Eqn.(2.4) and where $d[U]$ and $d[W]$ are, respectively, the integration measures for the gauge and Higgs fields. N_s denotes the number of sites on the lattice.

The first step in generating the approximation is to introduce a mean field action S_{MF} in which all non-local interactions are replaced by interactions with mean fields.

Inspection of Eqn.(2.4) suggests the following choice

$$\begin{aligned} S_{MF} &= \sum_{x,\mu} -\tfrac{1}{2} Tr\left[U^{\dagger}(x, x+\hat{\mu}) A(x, x+\hat{\mu})\right] \\ &+ \sum_{x} \lambda \left(\rho^2(x) - \gamma\right)^2 + 4\,\rho^2(x) \\ &+ \sum_{x} - \left(\tfrac{1}{2} Tr\left[W^{\dagger}(x) B(x)\right]\right) \end{aligned} \tag{4.3}$$

The fields $A(x, x+\hat{\mu})$ and $B(x)$ are the mean fields which simulate the influences on any given field of its neighbours. Both mean fields are chosen to be 2×2 complex matrices. Note also that the fields $\rho(x)$ appearing in the second line of Eqn.(4.3) are the Higgs radial fields introduced in Eqn.(3.7).

Given the mean field action S_{MF}, we can define the mean field expectation value $\langle O \rangle_{MF}$ of an operator O as follows

$$\langle\, O \,\rangle_{MF} = \frac{1}{Z_0(A,B)} \int \prod d[W] \prod d[U]\; O\; \exp\left(-S_{MF}\right) \tag{4.4}$$

where

$$Z_0(A,B) = \int \prod d[W] \prod d[U] \exp\left(-S_{MF}\right) \tag{4.5}$$

Then the partition function Z (Eqn.(4.2)) is given by

$$Z = Z_0\, \langle \exp\left(-S + S_{MF}\right) \rangle_{MF} \tag{4.6}$$

If we now apply the inequality of Eqn.(4.1) we find

$$Z \geq Z_0 \exp\left(-\langle S - S_{MF} \rangle_{MF}\right) \tag{4.7}$$

or in terms of the free energy per site

$$F \geq F_{MF}(A,B) = \frac{1}{N_s} \left(\ln\left(Z_0\right) - \langle S - S_{MF} \rangle_{MF}\right) \tag{4.8}$$

Eqn.(4.8) is the fundamental bound we require to generate the mean field approximation. The left hand side of this inequality is the free energy of the full theory. The right hand side is a lower bound for this free energy which depends on the arbitrary mean fields A and B. Thus, by maximizing F_{MF} with respect to A

and B, we can determine these mean fields as functions of the parameters in the theory.

In principle the best mean field approximation is obtained by maximizing F_{MF} over all possible choices for $A(x, x+\hat{\mu})$ and $B(x)$. Unfortunately such a procedure is much to difficult for our purposes. We shall instead adopt the following simplifying ansatz

$$A(x, x+\hat{\mu}) = a \begin{pmatrix} 1 & 0 \\ 0 & 1 \end{pmatrix} , \quad B(x) = b \begin{pmatrix} 1 & 0 \\ 0 & 1 \end{pmatrix} \tag{4.9}$$

where a and b are position independent constants. In this special case we find

$$\begin{aligned} F_{MF}(a,b) &= 24\,\beta\,[G'(a)]^4 + 4\,G'(a)\,[H'(b)]^2 \\ &+ 4\,[G(a) - aG'(a)] + [H(b) - bH'(b)] \end{aligned} \tag{4.10}$$

where $G(a)$ and $H(b)$ are defined by

$$\begin{aligned} G(a) &= \ln\left(\frac{2I_1(a)}{a}\right) \\ H(b) &= \ln\left(\frac{\int dr\, r^3\, \exp\left(-\lambda r^4 - (4-2\lambda\gamma)\, r^2\right)\ (2I_1(br)/br)}{\int dr\, r^3\, \exp\left(-\lambda r^4 - (4-2\lambda\gamma)\, r^2\right)}\right) \end{aligned} \tag{4.11}$$

F_{MF} is now a function of just two variables, and we shall need to find the pair of coordinates, $(a_{\max}, b_{\max})$, of the global maximum of F_{MF} as a function of the parameters β, λ, and γ, in order to determine the phase structure.

The results of the numerical determination of the mapping from parameter space to mean field maximum are plotted in Figure 2. This figure show the phase structure as a function of β and γ for $\lambda = 0.1$ and $\lambda = 1.0$. Solid lines represent first order transitions, and dashed lines represent second order transitions.

If we refer back to the results of Section 3 we can identify the origin of the various transitions shown in these figures. The first order transition occurring for γ negative separates phases with $a_{\max} = 0$ and $a_{\max} \neq 0$. The Higgs field maximum $b_{\max}$, however, remains constant ($b_{\max} = 0$) across the transition, and so is not actively participating in the physics of the transition. Further, we note that this is the region of the phase diagram where we expect the action to reduce to that of a pure $SU(2)$ gauge theory. Thus, the transition we are seeing is simply the

confinement-Coulomb phase transition which we expect to occur for pure $SU(2)$ gauge theories in all dimensions $d > 4$. For $d = 4$, though, we should be aware that this transition may be replaced by a crossover region, as occurs in the pure gauge theory.

The second order transition occurring for β large also has a simple explanation. Analysis of the data used to obtain the phase structure shows that the gauge mean field $a_{\max}$ remains constant across this transition, suggesting that the gauge fields are simply spectators in this transition. Also we note that this is exactly the region of parameter space where we expect the action to reduce to that of a pure Higgs theory. Thus, this transition appears to be a second order Higgs symmetry breaking transition. Also, in contrast to the gauge transformation discussed in the previous paragraph, we do expect this transition to be present when we analyze the Monte Carlo results, since the critical dimension for the Higgs symmetry breaking transition is $d = 2$.

The final transition line, occurring in the small β sector of the model's parameter space, is much more complicated. Both mean fields show significant change across this transition. Therefore, we must expect that both fields are actively participating in the dynamics of the transition. Furthermore, the data suggests that the transition in question appears to be a smooth continuation of both the second order Higgs symmetry breaking transition and the first order confinement-Coulomb transition. We interpret this transition, therefore, as a nontrivial combination of the other two transitions in the model. Also it is no longer clear whether or not this transition is a real feature of the model, since the obvious interplay between the gauge and Higgs sectors makes any predictions based on their separate properties impossible.

4.2 The Full Action in the Unitary Gauge

The discussion in Section 3 on Higgs-confinement complementarity has led us to expect that the model we are analyzing has only a single phase. We should therefore expect that the combination gauge-Higgs transition identified in Figure 2 is at least partially a mean field feature, since this transition does separate parameter space into two distinct phases. We have already identified one way this might occur.

Another possibility which we shall consider in this section concerns the presence of gauge degrees of freedom in the theory. The presence of such redundant degrees of freedom raises the possibility that those degrees of freedom may undergo a spurious transition which is not reflected in the physical observables. We shall therefore consider in this section how the results presented above change when the redundant degrees of freedom are integrated out.

The unitary gauge action is given in Eqn.(3.9). To generate a mean field version of this action we need to decide on appropriate forms for the mean fields to be introduced and for their interactions with the gauge and Higgs fields. The form which we have choosen is

$$\begin{aligned} S^{U}_{MF} &= \sum_{x,\mu} -\frac{1}{2} Tr\left[U^{\dagger}(x,x+\hat{\mu})A(x,x+\hat{\mu})\right] \\ &+ \sum_{x} \lambda\ \left(\rho^2(x)-\gamma\right)^2 + 4\,\rho^2(x) \\ &+ \sum_{x} -\rho(x)\ B(x) \end{aligned} \tag{4.12}$$

where $A(x,x+\hat{\mu})$ is a 2×2 complex matrix field, and $B(x)$ is now a one component real field. Note that the Higgs spin field $V(x)$ (Eqn.(3.7)) has dropped from the problem.

To determine the phase structure we need to maximize the mean field free energy with respect to the fields $A(x,x+\hat{\mu})$, and $B(x)$. As before we adopt the following ansatz to simplify this problem

$$A(x,x+\hat{\mu}) = a \begin{pmatrix} 1 & 0 \\ 0 & 1 \end{pmatrix}, \quad B(x) = b \tag{4.13}$$

where a and b are position independent constants. With these definitions, the only difference between the mean field free energy in the unitary gauge and that when no gauge is imposed is in the definition of the Higgs generating function H(b), which is now given by

$$H(b) = \ln\left(\frac{\int dr\ r^3\ \exp\left(-\lambda r^4-(4-2\lambda\gamma)\,r^2\right)\ \exp\left(br\right)}{\int dr\ r^3\ \exp\left(-\lambda r^4-(4-2\lambda\gamma)\,r^2\right)}\right) \tag{4.14}$$

The free energy itself takes exactly the form given in Eqn.(4.8). The change in the Higgs generating function, however, does markedly change the qualitative behaviour

of the mean field phase structure. The first effect is the disappearance of the second order Higgs symmetry breaking transition. This result is to be expected, since we understand this transition to be a bulk effect occurring for the Higgs spin degrees of freedom which have been integrated out in this gauge.

A more important result of the gauge choice is shown in Figure 3, which plots the Higgs mean field component of the global maximum of the free energy as a function of β for various values of γ. For γ small, these plots show a discontinuity in $b_{\max}$ as β increases. We interpret this discontinuity as evidence of the first order confinement-Coulomb transition which we have seen above. As γ increases however, the size of the discontinuity decreases and eventually disappears. Similar behaviour is seen when the Higgs mean field component is plotted against γ and the gauge field component is plotted against both β and γ.

The conclusions we draw from this behaviour are shown in Figure 4, which plots the phase structure for two different values of λ as predicted by the unitary gauge mean field approximation. The interesting feature to note is that, for $\lambda = 1.0$, the first order transition shown here does not separate the model parameter space into two phases. Rather, the transition line ends in the interior, and it is possible to move from any point in the parameter space to any other point without crossing a phase transition.

5 The Monte Carlo Method

Our basic aim in what follows will be to measure lattice expectation values of functions $O(U,W)$ of the gauge and Higgs fields by Monte Carlo methods [14] [15]. These expectation values are defined by the functional integral

$$\langle O(U,W)\rangle_S = \frac{\int \prod_{x,\mu} d[U(x,x+\hat{\mu})] \prod_x d[W(x)] \;\; O(U,W) \;\; \exp\left(-S\left(U,W\right)\right)}{\int \prod_{x,\mu} d[U(x,x+\hat{\mu})] \prod_x d[W(x)] \;\; \exp\left(-S\left(U,W\right)\right)} \tag{5.1}$$

The Monte Carlo approach approximates this integration by an average of $O(U,W)$ over a set of configurations $\{\{U,W\}_i\}$ of the fields $U(x,x+\hat{\mu})$ and $W(x)$,

which are chosen from the set of all possible configurations with a weight

$$P(\{U,W\}) \prod d[U] \prod d[W] = \frac{\prod d[U] \prod d[W] \exp(-S(U,W))}{\int \prod d[U] \prod d[W] \exp(-S(U,W))} \quad (5.2)$$

The utility of this approach is that it is possible to develop algorithms suitable for use on computers to generate appropriately distributed sets of configurations.

These Monte Carlo algorithms all follow the same general pattern. One first chooses some initial configuration $\{U,W\}_0$. Then one generates a sequence of new configurations $\{\{U,W\}_i, i = 0,\ldots\}$ iteratively. At each iteration step a new configuration is generated from the previous configuration by changing or "updating", one field at a time, some large subset of the fields of the old configuration.

There are two commonly used techniques to generate the sequence of configurations we need [15]. In the heat bath method, one chooses a new value for the field being updated with a weight proportional to $\exp(-S(\text{new}))$. This method produces a new value independent of the original field value, but of course dependent on its environment. In the standard Metropolis method, one first chooses a new value randomly from some subset of the possibilities. This new value is accepted unconditionally if it reduces the action of the configuration, but if the action is increased, then the new value is accepted only with a probability $\exp(-S(\text{new}) + S(\text{old}))$. The Metropolis updated variable depends both on its environment and on its previous value.

Numerically, the heat bath method is usually the harder to implement, but it has the advantage that the sequence of configurations it generates is usually significantly less correlated than a similar Metropolis generated sequence. For this reason, the extra effort involved in coding a heat bath scheme, if it is at all possible, is usually well justified, since fewer configurations are needed with the heat bath approach to generate results of a similar accuracy, and so simulation time is decreased.

For the action of Eqn.(2.4) we can divide the updates we need to do into two parts: the update of the gauge fields $U(x, x+\hat{\mu})$, and the update of the Higgs fields $W(x)$. $U(x, x+\hat{\mu})$ is an $SU(2)$ field and can be updated with the $SU(2)$ heat bath algorithm of Creutz [16]. Let us therefore consider the more difficult problem of implementing a heat bath algorithm for the Higgs field update. It is convenient first

to decompose $W(x)$ into its radial $\rho(x)$ and spin $V(x)$ degrees of freedom (Eqn.(3.7)). In order to update these fields at a site x, we need to generate new fields $\rho_n(x)$, and $V_n(x)$ with a weight

$$\begin{aligned} P(\rho_n(x),V_n(x)) \quad & \rho_n^3(x)d\rho_n(x) \quad d[V_n(x)] \\ \propto \quad & \exp\left(-S_H(\rho_n(x),V_n(x),E_H(x)) \right) \quad \rho_n^3(x)d\rho_n(x) \quad d[V_n(x)] \end{aligned} \tag{5.3}$$

where

$$\begin{aligned} S_H(\rho(x),V(x),E_H(x)) &= \lambda\,\rho^4(x) + (4-2\lambda\gamma)\,\rho^2(x) \\ &- \rho(x)\,\tfrac{1}{2}Tr\left[V^\dagger(x)E_H(x)\right] \end{aligned} \tag{5.4}$$

and

$$E_H(x) = \sum_\mu U(x,x\pm\hat{\mu})W(x\pm\hat{\mu}) \tag{5.5}$$

The function S_H appearing here is simply the set of terms in the action of Eqn.(2.4) which couple to the fields $\rho(x)$ and $V(x)$ which are being updated.

To generate variables according to a particular weight function, one generally must be able to invert the indefinite integral of the weight function. Unfortunately an analytic form for the indefinite integral of Eqn.(5.3) does not exist, and a numerical inversion is not feasable since the term in S_H (Eqn.(5.4)) which is linear in V has coefficients (E_H) which change every update and we would therefore need to calculate a new inversion table each update. This result is not really a surprise. Most interesting theories suffer the same problem, which is why Metropolis update schemes are so common in the literature of lattice gauge theories. In our case, however, it is not necessary to resort to the standard Metropolis scheme. We have instead used an alternative scheme which retains much of the flavour and advantages of a heat bath update [17].

In order to describe this scheme, we first rewrite the action S_H as follows

$$\begin{aligned} S_H(\rho,V,E_H) &= S_\rho^0(\rho) + S_V^0(V,E_H) + S_H^1(\rho,V,E_H) \\ S_\rho^0(\rho) &= \lambda\,\rho^4 + \kappa\,\rho^2 \\ S_V^0(V,E_H) &= -\alpha\,\tfrac{1}{2}Tr\left[V^\dagger E_H\right] \\ S_H^1(\rho,V,E_H) &= (4-2\lambda\gamma-\kappa)\,\rho^2 + (\alpha-\rho)\,\tfrac{1}{2}Tr\left[V^\dagger E_H\right] \end{aligned} \tag{5.6}$$

Notice that in splitting S_H into three pieces we have introduced two arbitrary constants κ and α.

The update algorithm which we shall use consists of the following steps. First the environment matrix E_H is calculated. Then new fields ρ_n and V_n are generated with weights

$$\begin{aligned} P_\rho(\rho_n)\ \rho_n^3 d\rho_n &= \exp\left(-S_\rho^0(\rho_n)\right)\ \rho_n^3 d\rho_n \\ P_V(V_n)\ d[V_n] &= \exp\left(-S_V^0(V_n, E_H)\right)\ d[V_n] \end{aligned} \tag{5.7}$$

Notice that the decomposition of S_H defined in Eqn.(5.6) together with the introduction of the constant α has enabled us to separate the generation of the Higgs radial and spin degrees of freedom.

Once the trial values ρ_n and V_n have been generated, we can correct for not including the term S_H^1 by doing a Metropolis-like acceptance test. The difference $\triangle S_H^1 = S_H^1(\rho_n, V_n, E_H) - S_H^1(\rho_o, V_o, E_H)$, where ρ_o and V_o are the old field values on the site being updated, is calculated. If $\triangle S_H^1 \leq 0$, then ρ_n and V_n are accepted automatically as the new field values. If, however, $\triangle S_H^1 \geq 0$, ρ_n and V_n are accepted only with probability $\exp(-\triangle S_H^1)$.

There are a number of interesting features to this algorithm. First, the new fields are chosen almost as if one is doing a heat bath update. All possibilites are considered, and serious consideration is given to the eventual desired distribution. In the standard Metropolis approach, one is usually forced to choose new trial fields by making a small perturbation on the old fields, which process further increases the correlations between configurations. The alternative of choosing new fields randomly from all the possibilities generally results in field values so far from equilibrium that they are seldom accepted.

A more important property to note is the fact that the algorithm satisfies detailed balance [15] independently of how one chooses the parameters α and κ. Thus, these variables can be chosen to maximize the ratio of new fields accepted to new fields rejected during the Metropolis test at the end of the update. Experimentally, the best choice for κ appears, not unexpectedly, to be that value which generates new fields ρ_n with an expectation $\langle \rho_n^2 \rangle_{S_\rho^0}$, which is equal to the full theory expectation value $\langle \rho^2 \rangle_S$ for the Higgs radial field ρ. α is determined by the choice $\alpha = \langle \rho \rangle_S$.

Both these choices require information which is not usually available at the beginning of a Monte Carlo. So at the start of a run, α and κ are estimated, and then as the run progresses and the required expectation values become available, the original estimates are adjusted.

6 Monte Carlo Results

We come now to the presentation of the numerical results we have obtained for the phase structure of the action of Eqn.(2.4). To keep things simple at first, we shall concentrate on the data we have obtained from simulations with the Higgs four-point coupling fixed at $\lambda = 0.1$. For this special case we shall discuss in some detail the evidence for the various transitions which are present. Later sections will present the phase picture for other values of λ. Finally, we shall discuss how these results compare with the mean field results obtained in Section 4.

Some of the results which we shall discuss here have been reported before in the literature. Lang, Rebbi and Virasoro [18] have performed simulations for the special case $\lambda = \infty$, where the radial Higgs field drops from the problem. Kuhnelt, Lang, and Vones [19] have identified the phase structure for λ large and observed no qualitative changes in the second order transition reported by the first group of authors.

6.1 Observables

One significant problem to be faced when one performs any lattice Monte Carlo simulation is the vast amount of data generated. For the case at hand, for example, if we choose to work on a 4×4 lattice, then each new configuration generates 5120 new numbers to be stored and analyzed. Since we expect, in the end, to have to examine hundreds of thousands of different configurations in order to extract the information we are searching for, it is apparent that only very limited data can be stored for each configuration. Generally, therefore, one chooses a few special operators or observables which are to be measured as the different configurations are generated, and once these measurements have been made the configuration

details can be discarded.

The operators we have chosen to use are defined as follows

$$\begin{aligned} O_S(U,V) &= \langle\, S(U,W)\,\rangle \\ O_U(U) &= \left\langle \left(1-\tfrac{1}{2}Tr\,[U_\Box]\right)\right\rangle \\ O_\rho(\rho) &= \left\langle\, \rho^2(x)\,\right\rangle \\ O_V(U,V) &= \left\langle \left(1-\tfrac{1}{2}Tr\left[V^\dagger(x)U(x,x+\hat\mu)V(x+\hat\mu)\right]\right)\right\rangle \\ O_L(U) &= \left\langle \tfrac{1}{2}Tr\left[\prod_{t=1}^{N_t} U\left((t,\vec x),(t+1,\vec x)\right)\right]\right\rangle \end{aligned} \tag{6.1}$$

where $U(x,x+\hat\mu)$, $\rho(x)$, and $V(x)$ are the gauge, the Higgs radial, and the Higgs spin fields, respectively, and where N_t denotes the number of sites in the time direction. One should note that these operators are not order parameters for the transitions discussed in Section 3. Indeed, Higgs-confinement complementarity is based on the observation that there are, in fact, no order parameters at all for this theory, and that in the end all the different phases will join smoothly onto each other. However, they do behave in some ways like order parameters, and do enable us to identify properties intrinsic to the different phases we are searching for.

Of the five operators we have introduced, the simplest is probably O_S. This operator measures the total action of a configuration, and is therefore the most significant signal of any interesting dynamics which may be occurring in a particular simulation. The operators, O_U, O_ρ, and O_V probe the gauge, the Higgs radial, and the Higgs spin sectors, respectively, of the theory. Note especially that each of these operators is gauge invariant. Finally O_L is the Wilson line operator for the gauge sector. This operator measures the free energy of an infinitely massive quark which couples only to the gauge sector of the theory [20].

If we recall for a moment the results of the mean field analysis of Section 4, then the reasons for our choice of operators becomes clear. Consider first the gauge sector crossover expected for γ negative (Section 3.2). To the left of this line, for β small, the gauge fields fluctuate wildly and we expect, therefore, that $O_U \to 1$. To the right, on the other hand, for β large, all the gauge matrices are close to the

identity, and therefore $O_U \to 0$. Thus, a change in O_U from a value close to one to a value close to zero suggests the presence of a gauge sector crossover.

The other well understood transition discussed in Section 4 is the Higgs symmetry breaking transition occurring for large β. In the symmetry broken phase, perturbation theory suggests that $O_\rho \propto \gamma$, and that $O_V \to 0$, since we expect the Higgs fields to sit at the bottom of the symmetry breaking potential with their spins aligned. If, on the other hand, the symmetry is unbroken, then there is no correlation between the spins on different sites, and we find $O_V \to 1$. Also, γ no longer sets the magnitude of the Higgs radial field, and O_ρ is therefore no longer proportional to that parameter. Thus, O_ρ and O_V both signal a Higgs symmetry breaking transition.

6.2 Phase Structure

The first step in determining the phase structure of our model is to search parameter space to identify those regions where critical slowing occurs in the Monte Carlo iteration procedure. Such slowing shows most easily in hysteresis plots [21] which are generated by first choosing some initial values for the parameters β, λ, and γ and then alternatively iterating the system and varying the parameters slightly until we have traced a path through parameter space to some final position and back again to the original starting point. If the path chosen happens to cross a phase transition then the slowing associated with the transition will cause a mismatch between the values of the observables as measured during the outgoing and the return journeys along the path. This mismatch is exactly the effect we need to search for.

Figure 5 shows the results of a representative sample of such searches at $\lambda = 0.1$. For reference we have also included the mean field predictions for the phase structure at this value of λ. In this figure the dotted lines represent those paths in parameter space which were studied for hysteresis effects. Solid lines represent those pieces of path for which a hysteresis signal was observed. The data used to generate this plot was obtained mostly on 4^4 lattices with some checks on 8^4 lattices. For the horizontal paths the step size choosen was $\triangle\beta = 0.2$. For the vertical paths the

step size was $\triangle\gamma = 0.25$. In each case we iterated 50 sweeps between steps. This is to be compared to a time of one to five sweeps required to equilibrate the system from a hot or cold start far from a transition.

Inspection of Figure 5 suggests that at $\lambda = 0.1$ there is a single line of phase transitions in the model which appears to completely separate the two phases present. This result is somewhat surprising in view of the expectations of Section 3 that the line of transitions which enters the plot at large β should end at some internal point of the plot. Note, however, that both mean field results also show completely separate phases at this value of λ. We conclude therefore that the limit $\beta \to 0$ discussed in Section 3.3 has real structure if λ is not too large.

Studies of the observables of Eqn.(6.1) at points removed from the transition provides us with further information about the nature of the physics involved. Consider first the horizontal portion of the Monte Carlo transition shown in Figure 5 which extends from $\beta \approx 3$ to the right hand edge of the plot. Above this line $O_V \sim 0$ and $O_\rho \sim \gamma$ indicating the presence of a broken symmetry Higgs sector. Below the line $O_V \sim 1$ and $O_\rho \sim 0$ indicating a symmetric Higgs sector. Also as we cross the transition we find very little variation in the value of O_U. This behaviour suggests that this portion of the transition is simply a symmetry breaking transition occurring within the Higgs sector of the theory and that the gauge sector is playing no part in the dynamics.

For the portion of the transition to the left of $\beta \approx 2$ things are more complicated. O_V and O_ρ still show behaviour characteristic of passage from a Higgs symmetric phase below the transition line to a Higgs symmetry broken phase above the line. However O_V now changes rapidly across the line indicating that the transition is no longer confined to just the Higgs sector.

Finally if we consider the portion of Figure 5 for $\gamma \leq 1$ we find that the Higgs observables show very little activity throughout this region of parameter space. O_U on the other hand behaves both qualitatively and quantitatively as for the pure $SU(2)$ system. In particular O_U exhibits a crossover from strong to weak coupling at $\beta \approx 2.2$. Note that this is the region where the mean field analysis predicts a first order transition. However because we are working in four dimensions we only

see the crossover remnant of this mean field transition in the full theory.

We can gain even further insight into the nature of the phase structure which we have found by studying the order of the phase transition shown in Figure 5. Figure 6 shows some of the results we have obtained from mixed-phase runs at $\lambda = 0.1$ [21]. Each point plotted here represents typically a thousand iterations on a 4×4 lattice. For β fixed and large the data shown suggests that O_V is a continuous function of γ. This behaviour is indicative of a second order transition. For β small, though, there appears to be a significant discontinuity present, indicative of a first order transition. These characteristic behaviours show also when the other observables are studied and when the data for each observable is replotted as a function of β.

The plot shown in Figure 7 provides further evidence for a first order transition in the small β sector. This plot shows the evolution of matched pairs of configurations as they switch parameters among themselves. The two sets of parameters used to generate this plot were $\beta = 1.3$, $\gamma = -2.4$, and $\beta = 1.4$, $\gamma = -2.4$. These values are quite close together, and are below that value of β where discontinuous behaviour is first observed (Figure 6). The dotted line which divides this plot identifies the point where the parameters are switched. This switch, however, has almost no effect on the values being measured, and we must conclude, therefore, that there are metastable states present, and that a first order phase transition is occurring.

Combining the results of the hysteresis searches and the mixed phase runs, we now conclude that, at $\lambda = 0.1$, the action of Eqn.(2.4) has a single line of phase transitions extending from $\gamma = 3.8$ for small β to $\gamma \approx 2.0$ for large β. For β small, we have good evidence that the transition is first order. For β large, on the other hand, there is no evidence of a first order transition in any of the studies we performed. We shall, therefore, identify the large β transition as a second order transition. However, note that we do not eliminate the possibility that this portion of the transition may, in fact, be weakly first order. Finally we note that the combination of first and second order transitions splits the plane of parameter space at $\lambda = 1$ into two separate phases.

Figure 8 shows the phase structure of our model for various values of λ. Each line in this plot was generated in a manner similar to that described above. As before,

solid lines represent first order transitions, while dashed lines represent second order transitions. The exact positions of the first order transitions was determined by the positions of the discontinuities associated with the presence of those transitions. For second order transitions when the hysteresis signal was large, the position could be found by first plotting the action as a function of γ with β and λ held fixed, and then identifying the position where this plot shows the greatest rate of change. For large values of λ, however, this procedure was not necessary, since the hysteresis signals there are not very wide, and provide a sufficiently accurate determination of the position of the transition.

Inspection of Figure 8 shows that, for $\gamma \geq 0.5$ the transition lines are all second order, and that each line terminates in the interior of the plot as the discussions of Section 3 have led us to expect. This particular region of parameter space is equivalent to that studied by Kuhnelt, et al., and the results we have presented here are in good agreement with the results reported by those authors.

For $\gamma \leq 0.2$, however, we see that some new physics is appearing. We find first that a section of the transition becomes first order. Then, as λ decreases even further, the transition end point moves to the $\beta = 0$ edge of parameter space, and the two phases present become disconnected. Another point to note about the structure at small λ is that the Monte Carlo data suggests that the changeover from first order to second order occurs at $\beta \approx 2.1$, independently of λ. This particular value of β is especially significant, since it also describes the crossover from strong to weak coupling behaviour in the pure $SU(2)$ gauge theory.

In Figure 9, we have redrawn the phase transitions for $\lambda = 0.1$ and $\lambda = 1.0$ together with the respective mean field predictions from Section 4. In each case we see that the combination gauge fixed and gauge unfixed mean field predictions agree quite well with the Monte Carlo result. In particular, the gauge fixed mean field results describe well the position of the transition which occurs at small β, while the gauge unfixed mean field results describe well both the position and the order of the large β Higgs symmetry breaking transition. Also note that the mean field results predict that the changeover in the order of the $\lambda = 0.1$ transition should occur at the same point as the strong to weak transition occurs in the pure $SU(2)$

mean field theory.

There are some interesting conclusions one can draw from the combination mean field and Monte Carlo results we have obtained. Firstly, for $\beta \geq 2.1$, we find that the gauge fields are all close to the identity and play no role in the the dynamics of the large β phase transition, which is, therefore, purely a Higgs sector phenomenon. For $\beta \leq 2.1$, however, both gauge and Higgs fields are actively involved in the transition. Further, both the mean field and Monte Carlo results suggest that, in this small β regime, the Higgs radial fluctuations play an important role in the transition, since when λ is large and the Higgs radial fluctuations are damped, we find that the transition extends only a short distance below $\beta = 2.1$. Finally we note that the mean field analysis has suggested a possible mechanism by which a single phase line can be be partially first order and partially second order. The mean field in fact predicts a triple point at the change in the order. Then, although the corrections to the mean field approximation introduced at four dimensions can eliminate one of the transitions defining this triple point, they do not necessarily eliminate the cooperative effects which seem to give rise to the the difference in order of the remaining two lines entering the triple point.

6.3 Finite Temperature Results

Let us turn now the finite temperature phase structure of the action of Eqn.(2.4). At this point we understand quite well this model's low temperature phase structure. Seemingly, there is just a single phase present, although, depending on one's choice of parameters, this phase can exhibit behaviour typical of either confinement or Higgs broken symmetry. At high temperatures we expect this picture to change. Thermal fluctuations should disrupt any long-range order associated with the Higgs symmetry breaking sector, and at high temperature the presence of a gluon plasma should cause deconfinement as in the pure gauge case.

We have already identified O_V and O_ρ as "order parameters" for the Higgs symmetry breaking transition. We need now to identify an operator sensitive to deconfinement due to the presence of a gluon plasma. In the pure $SU(2)$ gauge theory the relevant operator is the Wilson line operator O_L introduced in Eqn.(6.1).

We shall use O_L as a signal of gauge sector deconfinement for our model also, since, even in the presence of the Higgs fields, this operator still measures the free energy of an infinitely massive quark coupling only to the gauge degrees of freedom [20]. However it is important to realise that O_L is no longer an order parameter since the Z_2 symmetry [20], [22] which is probed by this operator in the pure gauge model is broken when fundamental Higgs fields are introduced. This feature is just one more consequence of the Higgs-confinement complementarity discussed in Section 3.

Having determined an appropriate set of observables, we can proceed with the finite temperature phase structure analysis. The fundamental ingredient for this analysis is the observation that a lattice with a finite extent in the time direction has a temperature T given by

$$T = \frac{1}{N_t\, a} \tag{6.2}$$

where N_t is the number of sites in the time direction and a is the lattice spacing [23]. The details of the Monte Carlo analysis follow exactly as above. We first try to identify the positions of all the transitions present by searching for hysteresis signals. Then, mixed phase techniques enable us to determine the orders of these transitions. Note, however, that since we are now also interested in how the phase structure changes as the temperature changes, we need to repeat this analysis for various different choices of N_t. The results which we shall present here were obtained from studies of $8^3 \times 2$, $8^3 \times 4$, $8^3 \times 6$, and $8^3 \times 8$ lattices.

If we confine our attention, at first, to the observables introduced in Section 6.1, then the Monte Carlo analysis on each of these new lattices produces a phase diagram exactly as in Figure 8. In particular, we note that there is no significant signal of N_t dependent shifts in any of the transitions shown there. This observation, of course, does not rule out the presence of such shifts, since they can be sufficiently small that they are masked by the inherent statistical uncertainties of the Monte Carlo process. This qualification of the Monte Carlo results which we have made is important because there is evidence from another source [24] which suggests that there might be small N_t dependent shifts in the position of the Higgs symmetry breaking transition. The analysis of reference [24] suggests that we should expect a shift of less than 5% in the position of the Higgs transitions on the $8^3 \times 2$ and $8^3 \times 8$

lattices. However, a 5% change in the position of the Higgs symmetry breaking transition is not sufficient to show above the Monte Carlo uncertainty, so we have no additional evidence for or against this shift.

Let us turn now to the results obtained from a study of the Wilson line operator, O_L. Figure 10 shows how O_L varies as a function of β at two different values of γ. This data was obtained from mixed phase studies on an $8^3 \times 2$ lattice with $\lambda = 0.1$. We see that, for each value of γ, the expectation value of O_L changes from small to large as β increases. Hysteresis studies show that in each case this changeover is associated with a definite hysteresis signal. For $\gamma = 6$, however, hysteresis also shows when the other observables are studied, and the position and abrupt nature of the change in O_L tells us that the transition involved is nothing more than the first order transition which we already know of from our analyses of those other observables.

For $\gamma = 0$, on the other hand, the hysteresis signals show only for O_L. There are no such signals when the other variables are studied. This behaviour is analogous to that which occurs at the deconfining transition in the pure gauge model. Note also that there is no longer any evidence of a discontinuous change in O_L as β increases. Thus we conclude that, at $\gamma = 0$, there is a second order deconfining transition similar to that which occurs in the pure gauge model.

Figure 10 shows only a small sample of the data we have obtained of the behaviour of O_L. One important feature of this data, however, is that for $\gamma \leq 2.0$ the values we obtain for O_L seem to be independent of γ and λ. This suggests that, as long as we remain in the symmetric Higgs phase, the gauge sector deconfining transition depends only weakly on these parameters. A comparison of the values obtained for O_L for the pure gauge theory with those obtained for the gauge-Higgs theory further reinforces this conclusion since the only distinguishable difference in the results of the two models is that in the confined sector of the gauge-Higgs model ($\beta < 1.5$ in Figure 10) O_L is close to but not identically zero as it is required to be in the pure gauge theory. We understand this shift as being due to the presence of charged Higgs which can screen a bare fermion. However the fact that the shift in O_L is so small, together with the good agreement between the pure gauge model

and the combined gauge-Higgs model for $\gamma < 2.0$, suggests that in this sector the Higgs is very massive and is therefore decoupling.

Figure 11 shows how the $\gamma = 0$ data of Figure 10 changes as the lattice size changes. We see that the position of the deconfining transition appears to be dependent on the lattice extent in the time direction. Hysteresis analyses and similar studies at other values of γ and λ confirm this observation, and we find that the deconfining transition shown in Figure 12 moves to larger values of β as N_t increases but is otherwise unchanged. Once again we find that the position of the transition appears to be independent of γ and λ.

This N_t dependent behaviour is very reminiscent of that observed for the pure gauge theory, and suggests that we can define a transition temperature $T_c = (N_t a)^{-1}$ which will remain constant as N_t increases provided that we scale the parameters appropriately. The hard part in implementing this suggestion, of course, is to determine exactly how β, λ and γ should scale. However, because the position of the transition is apparently independent of λ and γ, it is clear that β is the only parameter which is constrained when we require T_c to be independent of a. Consider, therefore, the renormalization group equation which defines T_c in terms of the critical coupling β_c in the pure gauge theory [22]

$$T_c = \frac{\Lambda}{N_t} \exp\left(\frac{2\pi^2\beta_c}{b_0}\right) \tag{6.3}$$

If we assume that β is the only relevant parameter then a similar equation applies in the full theory. The only differences that arise are in the numerical values of the constant b_0. For the pure gauge theory $b_0 = 44/6$, while for the combined gauge-Higgs theory $b_0 = 41/6$. We find that the numerical data is quite consistent with either scaling behaviour. However the discussions above suggest that the more probable explanation of this phenomenon is that the scaling is pure gauge and that the Higgs decouples as we take $a \to 0$ with γ and λ held fixed.

Analyses similar to those shown in Figure 11 at other values of γ and λ generate the phase structure shown in Figure 12. The vertical dotted lines in this figure show how the second order deconfining transition we have just identified behaves as the parameters are varied. The other structure shown is already familiar from Figure 8.

There are two different features of this plot which need further comment. Firstly, as we have already noted, the Monte Carlo data does not show any significant shifts in the position of the second order transition as λ is varied. Thus, the different vertical lines should really lie on top of each other. We have separated them slightly, however, to make the details more clear. Secondly, the exact structure at the different triple points shown is only tentative, since close to these points all the observables show interesting structure and it is therefore very difficult to identify exactly what is happening.

7 Conclusions

We have presented Monte Carlo and mean field results for the phase structure of an $SU(2)$ gauge-Higgs system. For fixed Higgs four point coupling this model has a single phase transition line which appears to be second order in the weak gauge coupling sector. However, in the strong gauge coupling sector this phase transition line can become first order. The fact that the phase transition is second order for at least part of its length is encouraging since it allows for the possibility that an appropriate scaling of the parameters as $a \to 0$ will produce a real continuum theory. Two obvious candidates for the continuum theory which might result are the Weinberg-Salam-Glashow model of the weak interactions with the fermions and $U(1)$ gauge sectors turned off, and the strong coupling Abbot-Farhi model.

When finite temperature effects are considered, we have identified an extra transition in the theory. This transition corresponds to the deconfinement transition in the pure gauge model and as long as we remain within the Higgs symmetric phase of the gauge-Higgs model this transition appears to be independent of the Higgs sector. We conclude that the Higgs decouples very rapidly in this sector of the full theory. This result is of interest to current studies of $SU(3)$ systems with dynamical fermions since it provides a warning that some considerable care might be needed in order to arrange that the fermions introduced into these systems remain dynamical when renormalization effects are included.

ACKNOWLEDGEMENTS

The author would like to thank N. H. Christ for his constant help and encouragement throughout the course of this work. Also many useful conversations with A. E. Terrano and O. Martin are gratefully acknowledged. This work was supported in part by the U.S. Department of Energy.

After the calculations reported here were completed, we received a preprint by J. Jersak, C.B. Lang, T. Neuhaus, and G. Vones [25] which presents Monte Carlo results on the zero temperature phase structure of the gauge-Higgs model. We find that we are in good agreement with the results of these authors.

REFERENCES

1. N. H. Christ and T. E. Terrano, Columbia University preprint CU-TP-325 (1985);
   S. A. Gottlieb, J. Kuti, D. Toussaint, A. D. Kennedy, S. Meyer, B. J. Pendleton, and R. L. Sugar, USCD preprint USCD-10P10-250 (1985)

2. B. Svetitsky and F. Fucito, Phys. Lett. 131B (1983) 165;
   T. Celik, J. Engels, and H. Satz, Phys. Lett. 129B (1983) 323;
   J. Kogut, H. Matsuoka, M. Stone, H. W. Wyld, S. Shenker, J. Shigemitsu and D.K.Sinclair, Phys. Rev. Lett. 51 (1983) 869

3. H. Hamber and G. Parisi, Phys. Rev. Lett. 47 (1981) 1792;
   E. Marinari, G. Parisi, and C. Rebbi, Phys. Rev. Lett. 47 (1981) 1975

4. S. Gottlieb, P. B. Mackenzie, H. B. Thacker, and D. Weingarten, FERMILAB preprint 84/98-T (1984)

5. D. J. Gross and F. Wilczek, Phys. Rev. D8 (1973) 3633

6. H. B. Nielson and M. Ninomiya, Nucl. Phys. B185 (1980) 20;
   Nucl. Phys. B195 (1982) 541;
   N. Kawamoto and J. Smit, Nucl. Phys. B192 (1982) 541

7. S. L. Glashow, Nuc. Phys. 22 (1961) 579;
   S. Weinberg, Phys. Rev. Lett. 19 (1967) 1264; Phys. Rev. D5 (1972) 1412;
   A. Salam, in Elementary Particle Theory, ed. N. Svartholm, Stockholm, 1968, p.361;
   S. L. Glashow, J. Iliopoulos, and L. Maiani, Phys. Rev. D2 (1970) 1285

8. L. F. Abbott and E. Farhi, Phys. Lett. 101B (1981) 69;
   Nucl. Phys. B189 (1981) 547

9. G. S. Rushbrooke, G. A. Baker and P. J. Wood in Phase Transitions and Critical Phenomena, Vol. 3, ed. C. Domb and M. S. Green

10. J. Frolich and B. Simon, Comm. Math. Phys. 50 (1976) 79

11. M. Creutz, Phys. Rev. Lett. 43 (1979) 553

12. E. Fradkin and S. H. Shenker, Phys. Rev. D19 (1979) 3682

13. R. Balian, J. M. Drouffe and C. Itzkyson, Phys. Rev. D10 (1973) 3376;
J. M. Drouffe and J. B. Zuber, Phys. Rep. 102 (1983) 1

14. N. Metropolis, et al., J. Chem. Phys. 21 (1953) 1087

15. K. Binder in Monte Carlo Methods in Statistical Physics, ed. K. Binder,
Springer-Verlag (1979), p. 1

16. M. Creutz, Phys. Rev. D21 (1980) 2308

17. B. Freedman, P. Smolensky, and D. Weingarten, Phys. Lett. 113B (1982) 481

18. C. B. Lang, C. Rebbi and M. Virasaro, Phys. Lett. 104B (1981) 294

19. H. Kuhnelt, C. B. Lang, G. Vones, Nucl. Phys. B230 [FS10] (1984) 16

20. L. D. McLerran and B. Sevtitsky, Phys. Rev. D24 (1981) 450

21. C. Rebbi, Phys. Rev. Lett. 43 (1979) 553

22. L. D. McLerran and B. Sevtitsky, Phys. Lett. 98B (1981) 195;
J. Kuti, J. Polonyi and K. Szlachanyi, Phys. Lett. 98B (1981) 199

23. C. W. Bernard, Phys. Rev. D9 (1974) 3312

24. R. C. Brower, D. A. Kessler, T. Schalk, H. Levine, and M. Nauenberg,
Phys. Rev. D25 (1982) 3391

25. J. Jersak, C. B. Lang, T. Neuhaus, and G. Vones, Aachen preprint
PITHA 85/05 (1985)

FIGURE CAPTIONS

1. Phase structure suggested by the analysis of Section 3. The dashed portion of the transition shown is an extrapolation.

2. Mean field prediction for the phase structure of the gauge-Higgs model for two different values of λ when no gauge fixing is imposed. Solid lines represent first order transitions. Dashed lines represent second order transions. Also indicated are the values which the mean fields achieve in each sector.

3. The value of the Higgs mean field $b_{\max}$ which maximizes the unitary gauge mean field free energy plotted as a function of β for various values of γ.

4. Mean field prediction for the phase structure of the gauge-Higgs model for two different values of λ in the unitary gauge. The solid lines shown represent first order transitions.

5. Results of hysteresis studies at $\lambda = 0.1$ on 4^4 and 8^4 lattices. Dotted lines show those paths which were studied. Solid lines show where a positive hysteresis effect was seen. For reference the mean field results for no gauge fixing (MF1) and for the unitary gauge (MF2) are also plotted.

6. Results of mixed phase studies at $\lambda = 0.1$. Each point shown represents the average of the operator O_V of approximately 1000 sweeps.

7. Evolution of the operator O_V for two different values of β. At the vertical dashed line the values of β used to evolve each configuration are swapped.

8. Monte Carlo predictions for the phase structure of the gauge-Higgs model. Solid lines represent first order transitions. Dashed lines represent second order transitions.

9. Comparisons of the Monte Carlo (MC), the mean field with no gauge fixing (MF1), and the gauge fixed mean field results (MF2) for two different values of λ.

10. Results of mixed phase studies of the operator O_L at $\lambda = 0.1$ on an $8^3 \times 2$ lattice.

11. Results of mixed phase studies of the operator O_L at $\lambda = 0.1$ and $\gamma = 0.0$ on $8^3 \times 2$, $8^3 \times 4$, $8^3 \times 6$, and $8^3 \times 8$ lattices.

12. Finite temperature phase structure for two different values of λ. Solid lines represent first order transitions. Dashed lines represent second order transitions. The new feature appearing in this diagram in the vertical second order gauge deconfinement transition (dotted line) identified by the Wilson line operator. This transition is a temperature dependent feature. This figure shows how this line moves as we go from an $8^3 \times 2$ lattice to an $8^3 \times 8$ lattice.

Figure 1

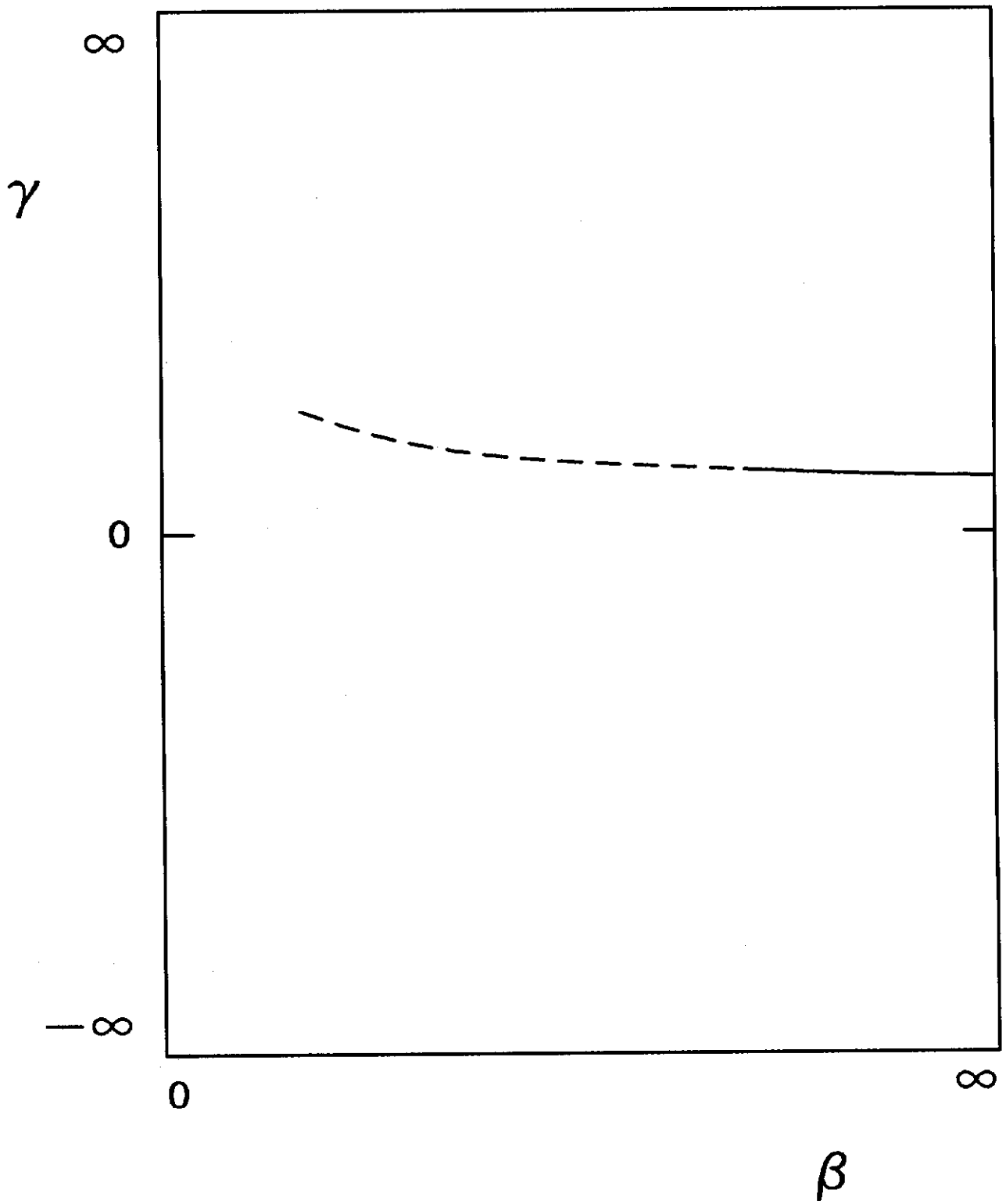

Figure 2

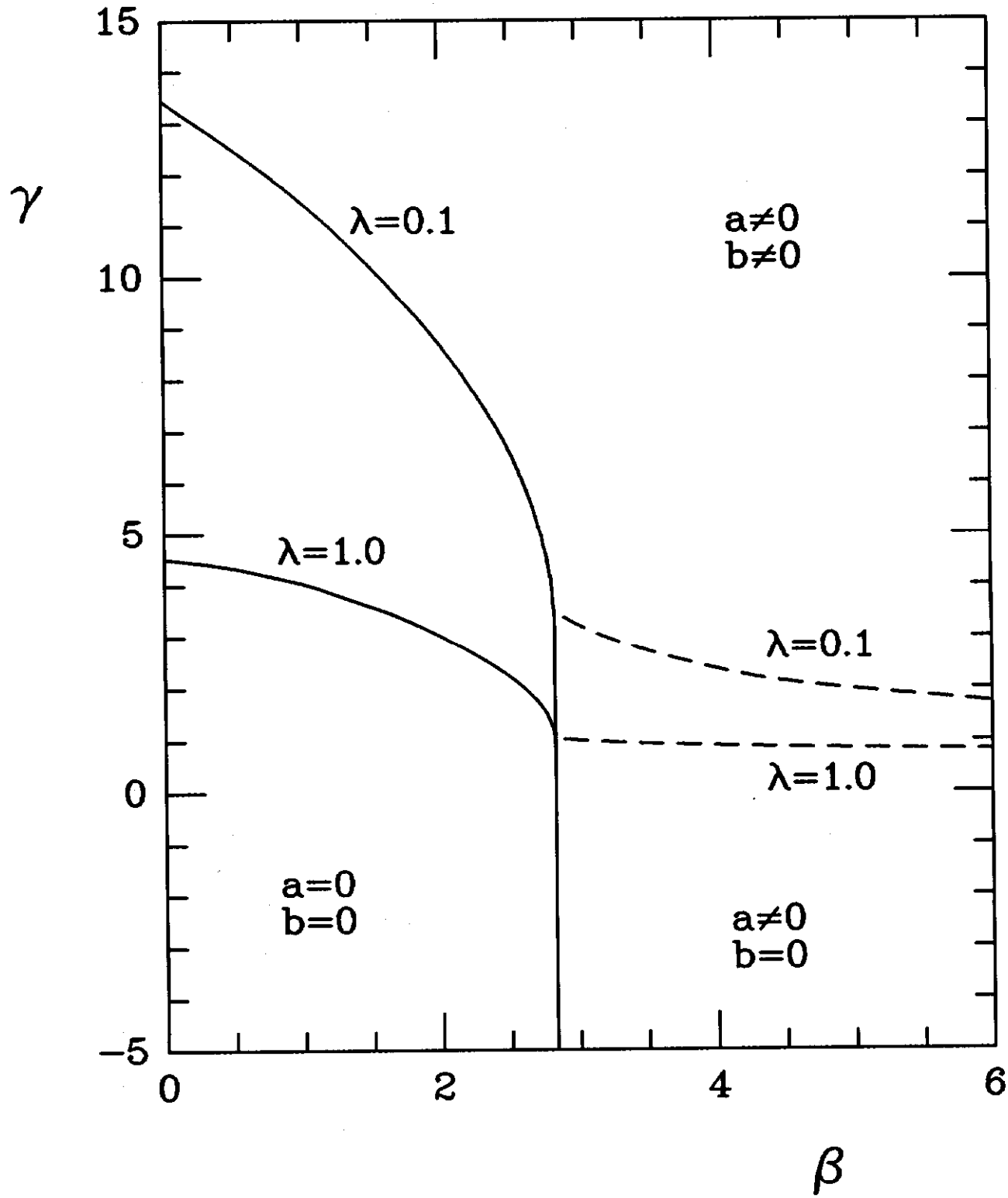

Figure 3

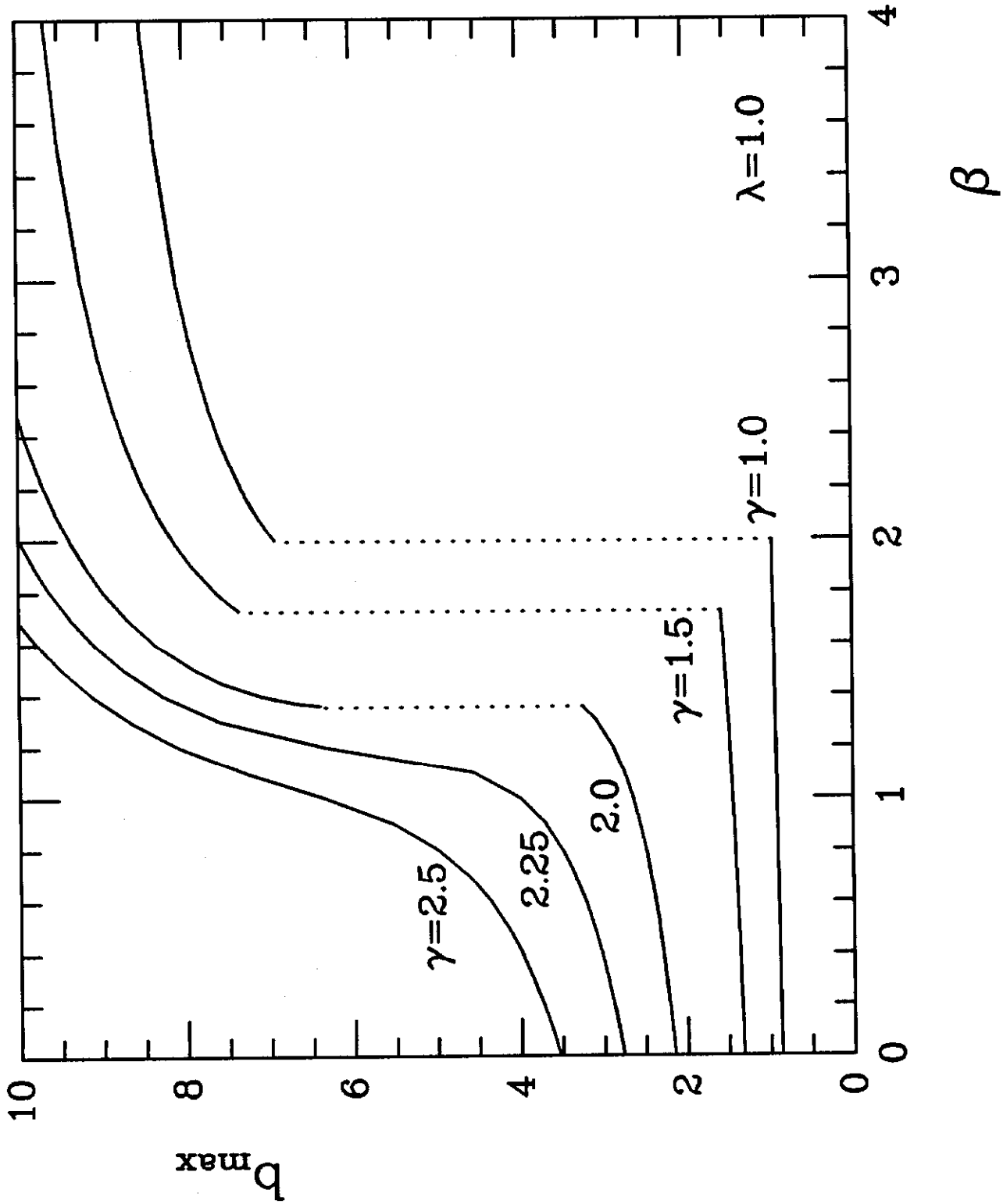
b_{max}
β
λ=1.0
γ=1.0
γ=1.5
2.0
2.25
γ=2.5
0
2
4
6
8
10
0
1
2
3
4

Figure 4

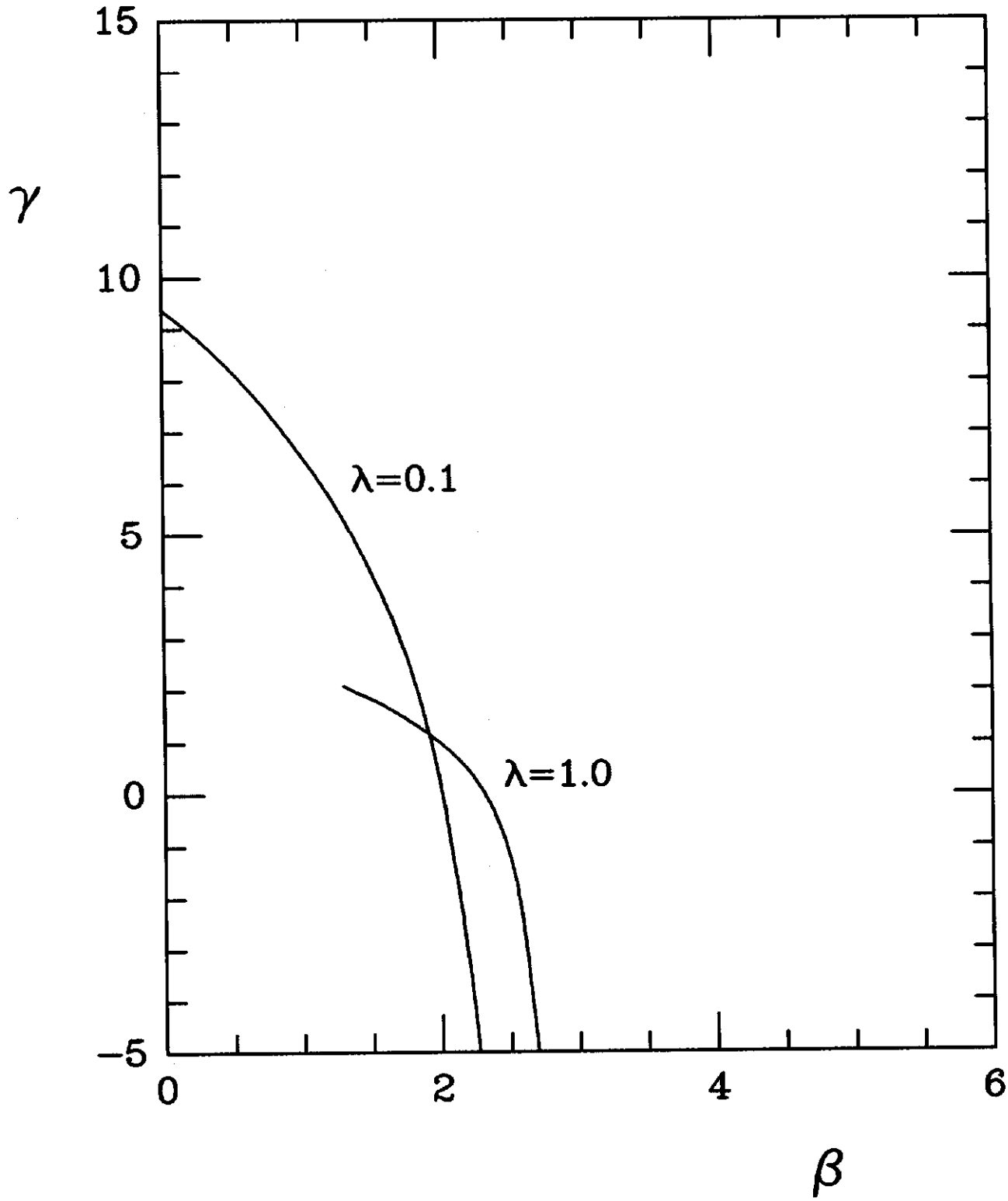

Figure 5

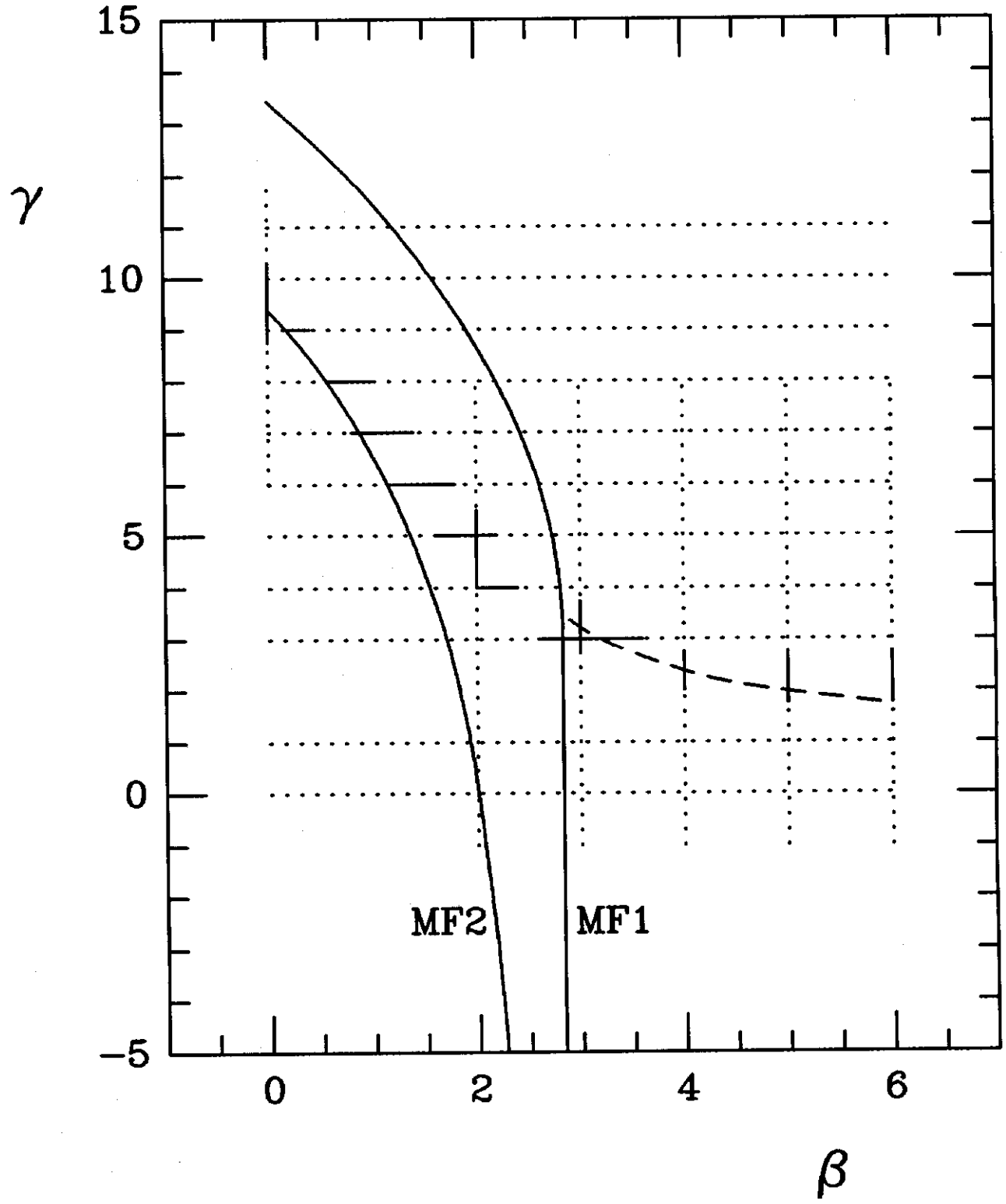

Figure 6

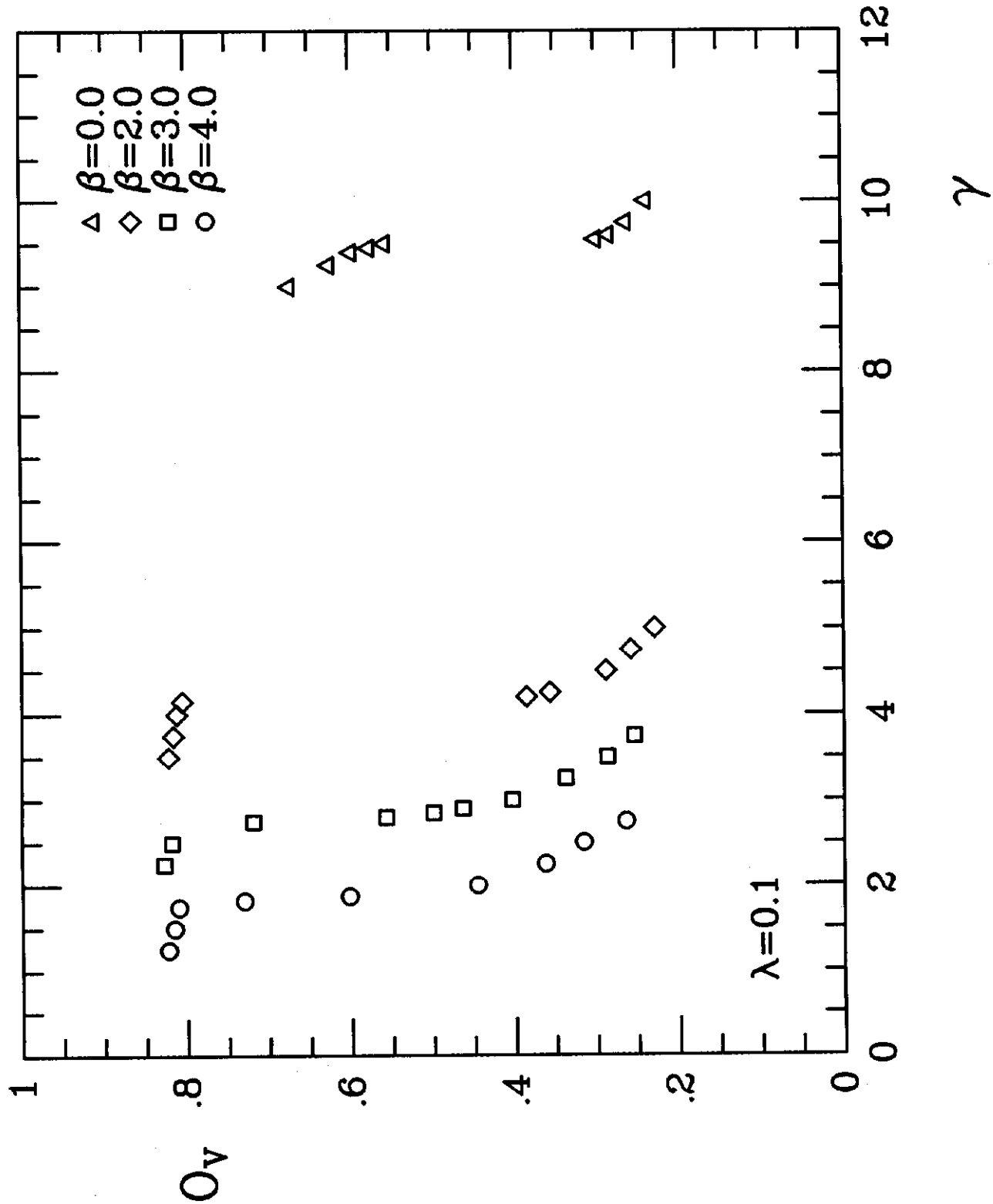

Figure 7

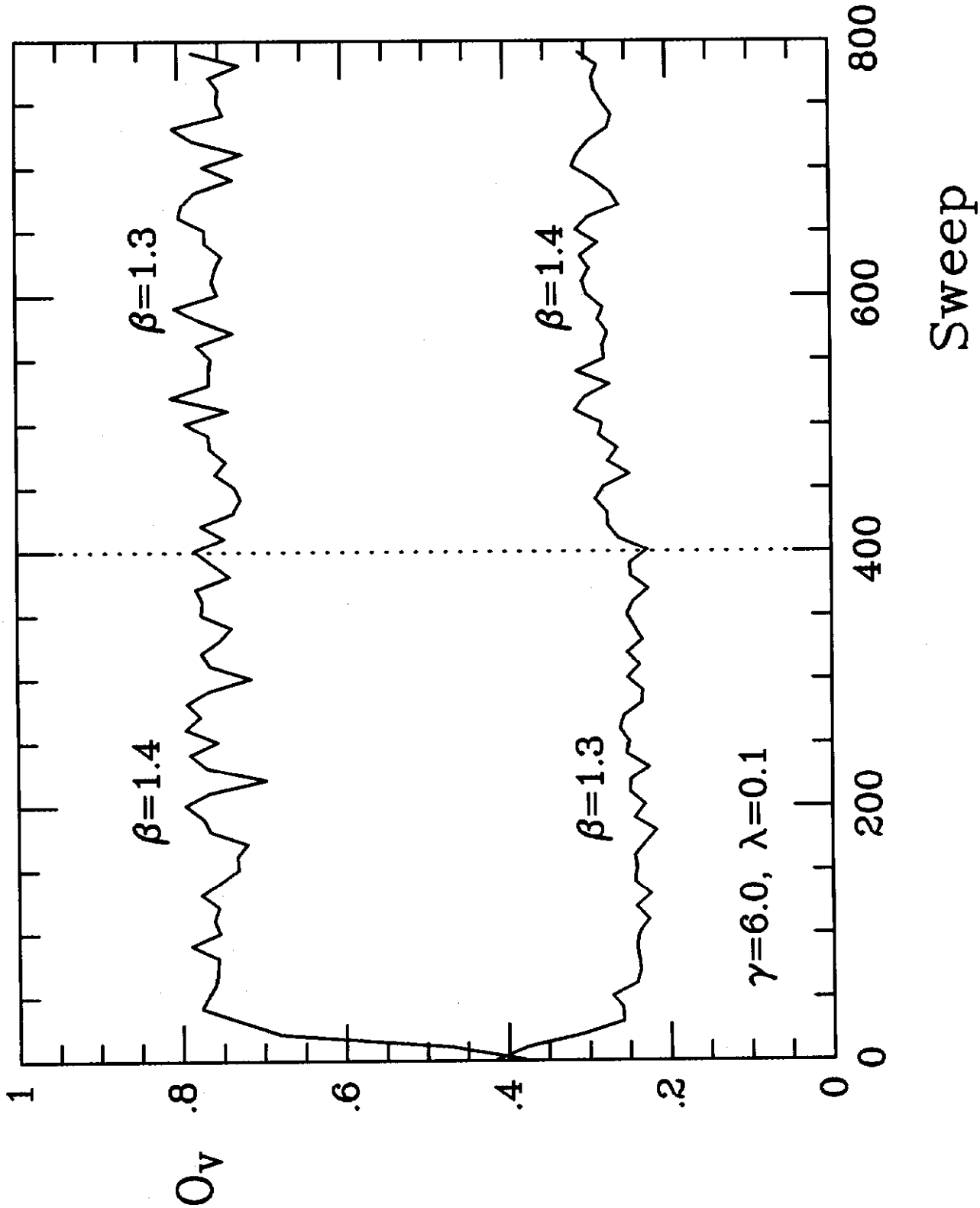

Figure 8

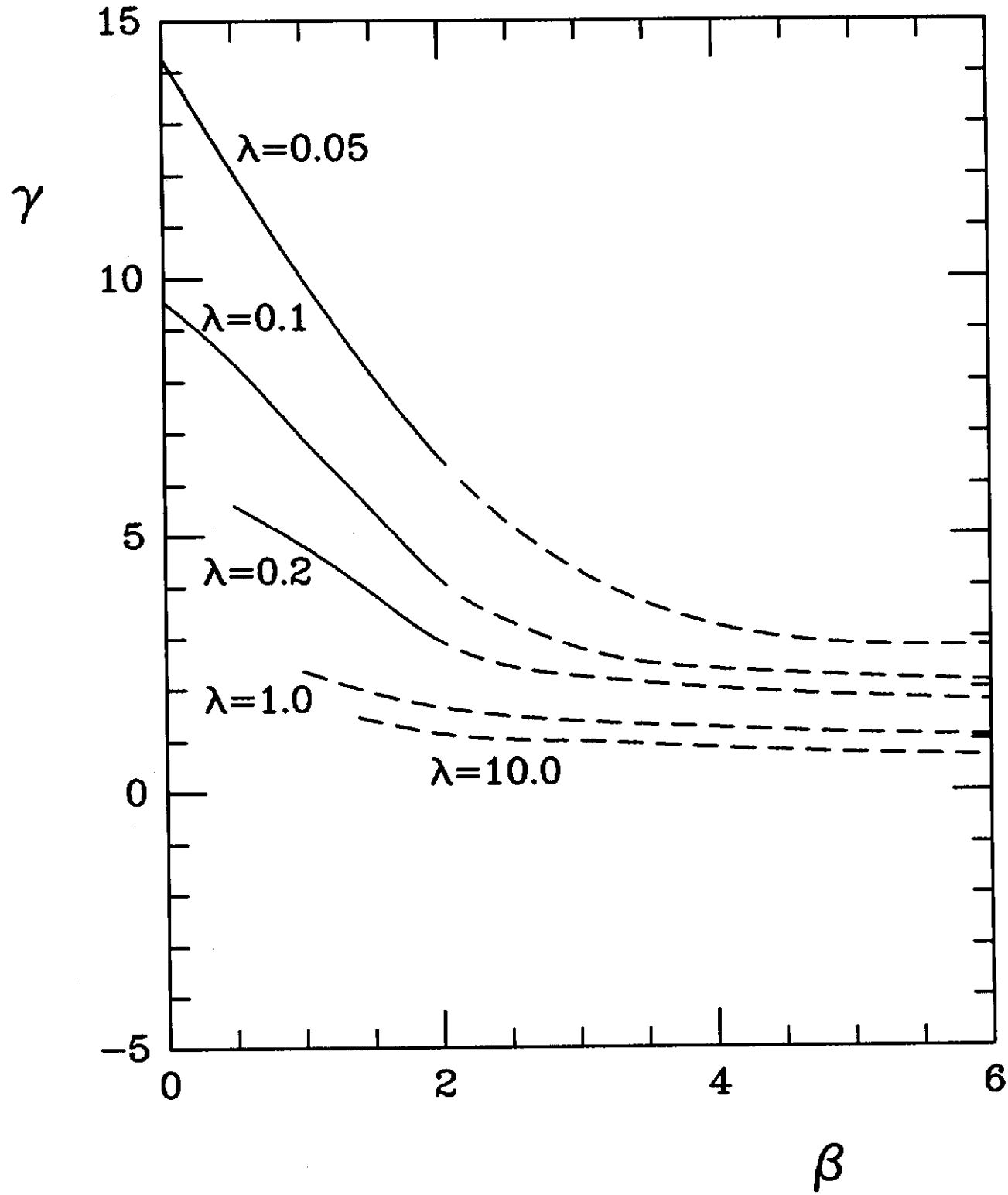

Figure 9a

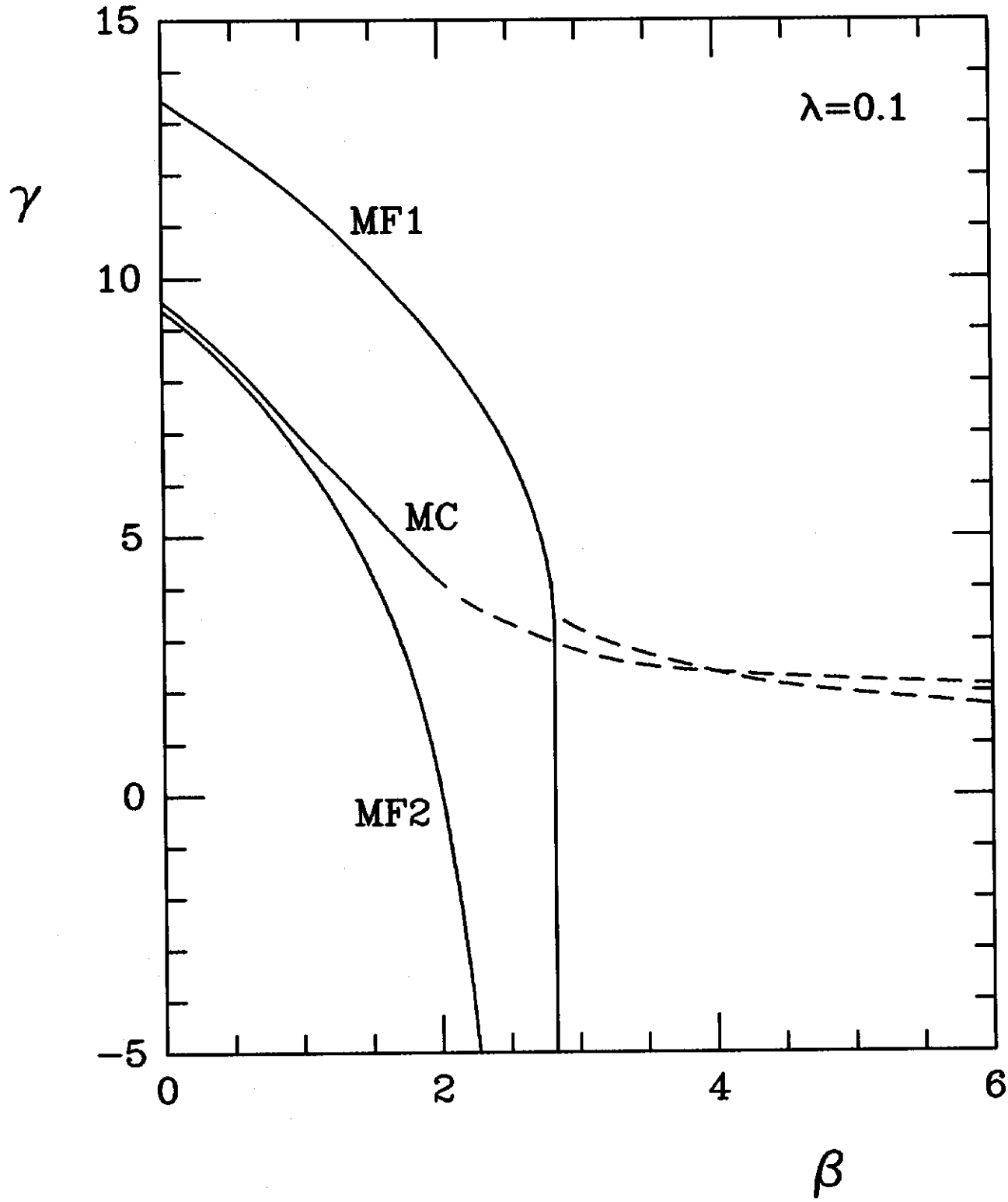

Figure 9b

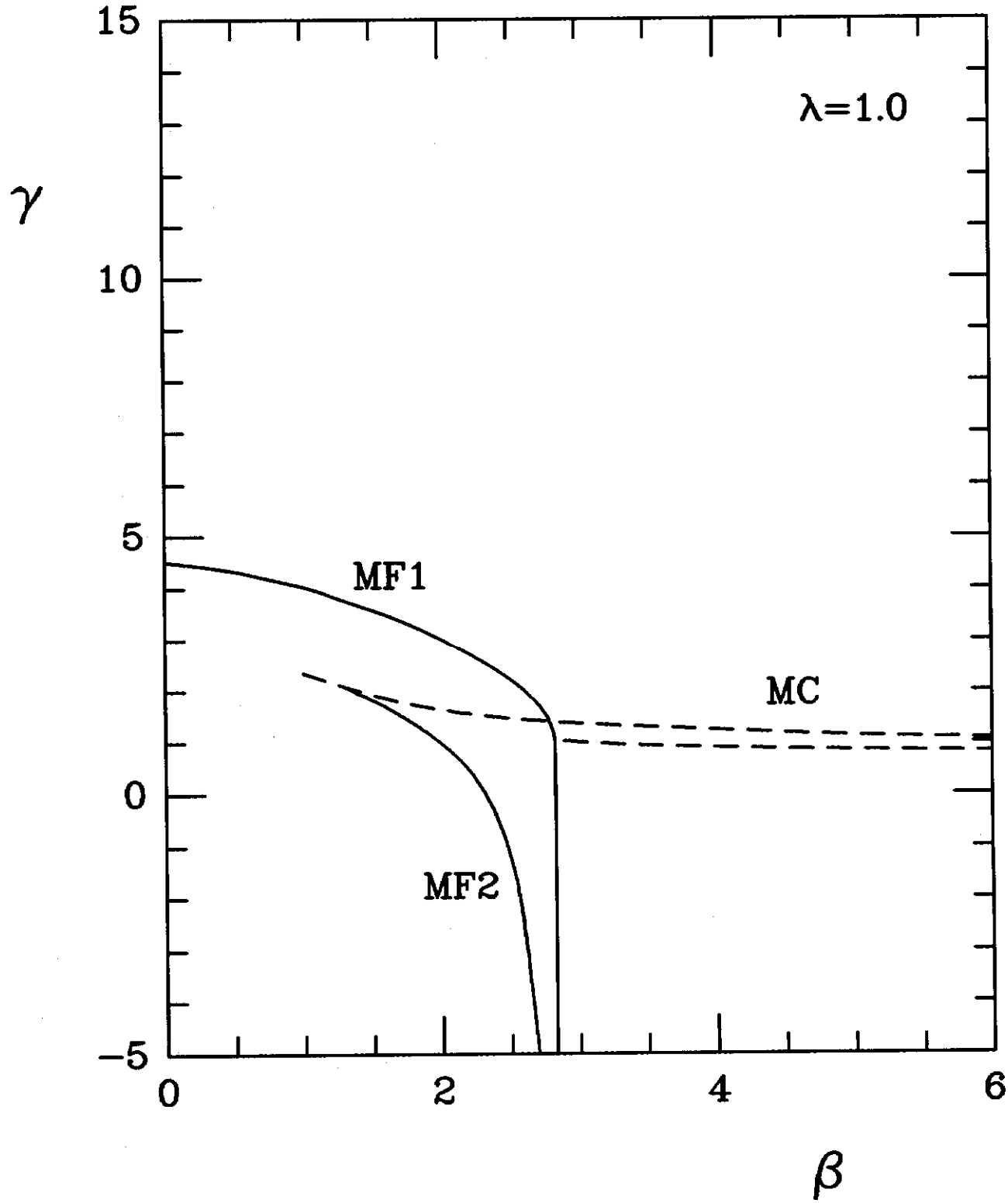

Figure 10

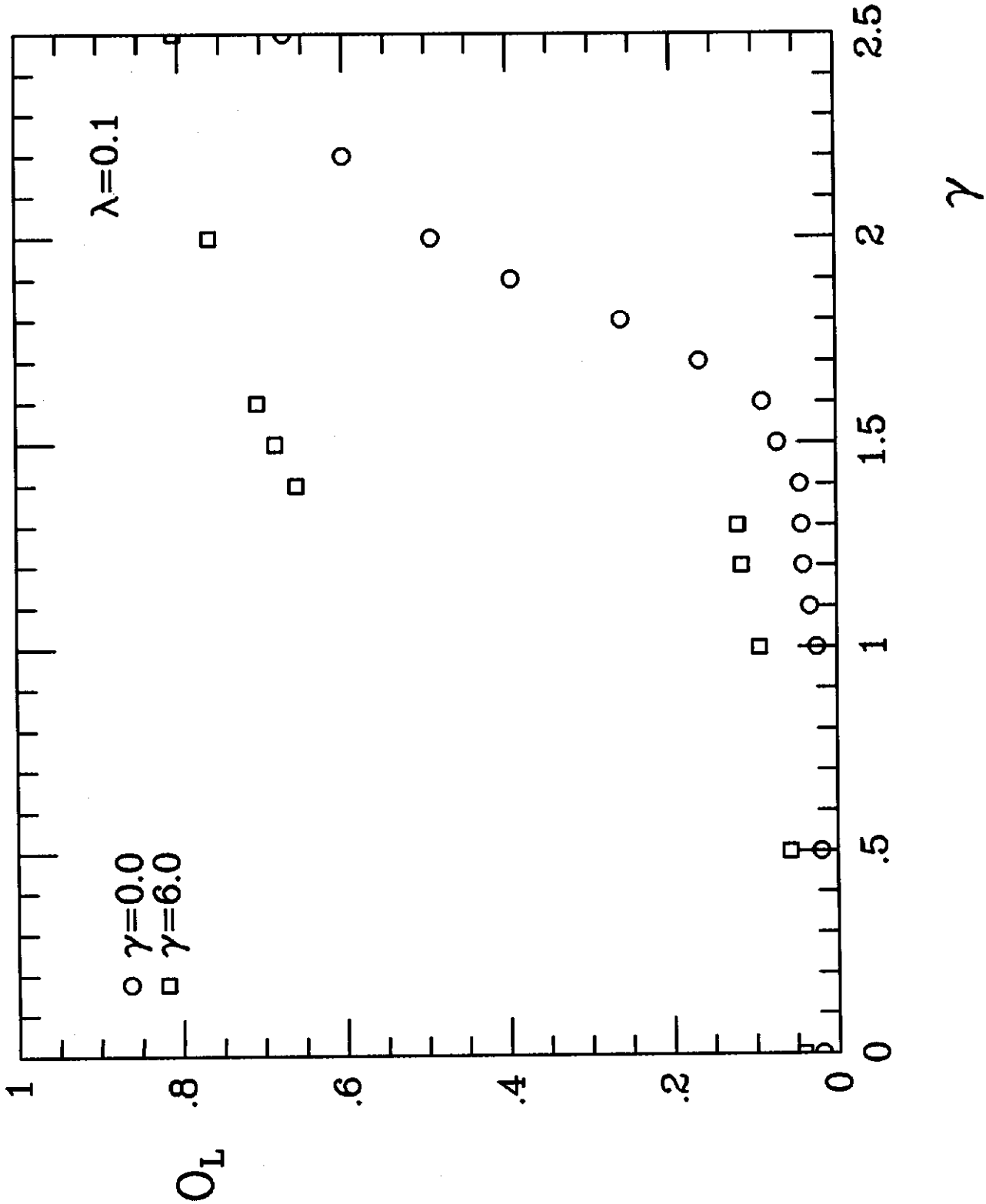

Figure 11

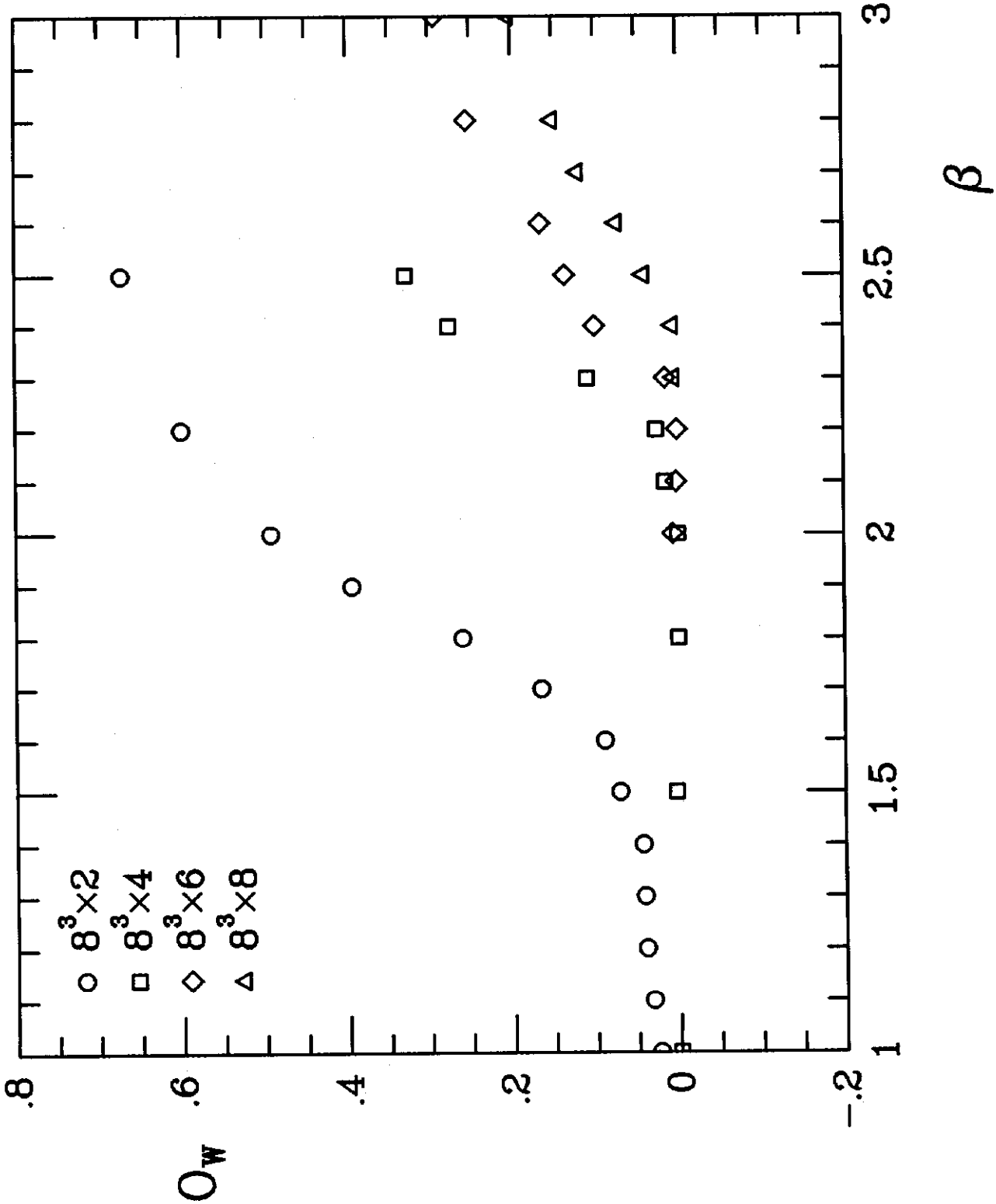
O_W
.8
.6
.4
.2
0
-.2
3
2.5
2
1.5
1
β
$8^3\times2$
$8^3\times4$
$8^3\times6$
$8^3\times8$

Figure 12